PNAS RESEARCH ARTICLE | IMMUNOLOGY AND INFLAMMATION OPEN ACCESS

RORγt-expressing dendritic cells are functionally versatile and evolutionarily conserved antigen-presenting cells

Hamsa Narasimhan[a,b], Maria L. Richter[c], Ramin Shakiba[a,b], Nikos E. Papaioannou[b,1], Christina Stehle[d], Kaushikk Ravi Rengarajan[a,b], Isabel Ulmert[e], Arek Kendirli[f,g,h], Clara de la Rosa[f,g,i], Pin-Yu Kuo[a,b], Abigail Altman[j,k], Philipp Münch[l], Saba Mahboubi[l], Vanessa Küntzel[b], Amina Sayed[a], Eva-Lena Stange[m], Jonas Pes[m], Alina Ulezko Antonova[n], Carlos-Filipe Pereira[j,k], Ludger Klein[a], Diana Dudziak[o], Marco Colonna[n], Natalia Torow[m,2], Mathias W. Hornef[m], Björn E. Clausen[l], Martin Kerschensteiner[f,g,h], Katharina Lahl[e,p,q,r], Chiara Romagnani[d], Maria Colomé-Tatché[c], and Barbara U. Schraml[a,b,3]

Affiliations are included on p. 11.

Edited by Hongbo Chi, St Jude Children's Research Hospital, Memphis, TN; received August 28, 2024; accepted January 13, 2025 by Editorial Board Member Warren J. Leonard

Conventional dendritic cells (cDCs) are potent antigen-presenting cells (APCs) that integrate signals from their environment allowing them to direct situation-adapted immunity. Thereby they harbor great potential for being targeted in vaccination, autoimmunity, and cancer. Here, we use fate mapping, functional analyses, and comparative cross-species transcriptomics to show that RORγt$^+$ DCs are a conserved, functionally versatile, and transcriptionally distinct type of DCs. RORγt$^+$ DCs entail various populations described in different contexts including Janus cells/RORγt-expressing extrathymic Aire-expressing cells (eTACs), subtypes of Thetis cells, RORγt$^+$-DC (R-DC) like cells, cDC2C and ACY3$^+$ DCs. We show that in response to inflammatory triggers, RORγt$^+$ DCs can migrate to lymph nodes and in the spleen can activate naïve CD4$^+$ T cells. These findings expand the functional repertoire of RORγt$^+$ DCs beyond the known role of eTACs and Thetis cells in inducing T cell tolerance to self-antigens and intestinal microbes in mice. We further show that RORγt$^+$ DCs with proinflammatory features accumulate in autoimmune neuroinflammation in mice and men. Thus, our work establishes RORγt$^+$ DCs as immune sentinel cells that exhibit a broad functional spectrum ranging from inducing peripheral T cell tolerance to T cell activation depending on signals they integrate from their environment.

dendritic cells | RORγt | AIRE | innate lymphocytes | antigen presenting cells

Significance

Antigen-presenting cells (APCs) orchestrate T cell immunity. Retinoic acid receptor-related orphan receptor-γt (RORγt)-expressing APCs are heterogenous regulators of T cell tolerance but their subtypes and lineage relationships are ill-defined. We report that RORγt$^+$ dendritic cells (DCs) are evolutionarily conserved, exhibit wide tissue distribution and reconcile various RORγt$^+$ APC populations known to promote peripheral T cell tolerance. We show that RORγt$^+$ DCs can sense pathogens, migrate to lymph nodes, activate naïve CD4$^+$ T cells, and accumulate in demyelinating neuroinflammation with a proinflammatory phenotype. Thus, RORγt$^+$ DCs have a broad functional spectrum ranging from inducing T cell tolerance to T cell activation depending on signals they integrate from their environment. This highlights their therapeutic potential and their affiliation with DCs.

cDCs are immune sentinels located in lymphoid and nonlymphoid tissues (1–3). They effectively sense pathogens and subsequently migrate to and initiate T cell responses in secondary lymphoid organs (1–3). Their functional versatility makes them attractive for being targeted in autoimmunity and vaccination against pathogens or cancer (2–5). Accordingly, considerable work has been invested in understanding the functional and ontogenetic diversity of cDCs, yet these cells remain ambiguous to define as fate mapping has recently uncovered novel populations with overlapping phenotype but distinct origin (2, 6–11).

Type 2 cDCs (cDC2) are potent regulators of CD4$^+$ T cell responses (1–3) that entail Notch2-dependent ESAM^{high} or T-bet-expressing cDC2A and Notch2-independent ESAM^{low} or T-bet-negative cDC2B that derive from myeloid progenitors (12–14). Both subtypes can induce Th17 responses but cDC2A regulate T follicular helper cell (Tfh) responses (15), while cDC2B may better promote Th2 responses (16). Recently, fetal liver lymphoid progenitors and lymphoid-derived transitional DCs (tDCs) have been shown to differentiate into cells resembling cDC2A and cDC2B (8–10, 17), the functional consequences of which are still unclear. tDCs can also contribute to antiviral responses and inflammation induced-immunopathology (8, 9, 17). Additionally, DC3 arise from monocytic progenitors, resemble cDC2B but in vitro appear superior to cDC2B in polarizing producing Th17 cells (11, 18, 19). The above heterogeneity suggests a careful division of labor between DC subtypes which needs to be better defined to uncover the full functional spectrum of cDCs.

Next to cDCs, RORγt-expressing APCs have emerged as potent regulators of T cell–mediated tolerance (20–30). RORγt is a ligand-activated transcription factor encoded by the *Rorc* gene that differs from its isoform RORγ by three amino acids at the amino terminus (31–33). RORγt-expressing APCs include subsets of ILC3s, RORγt$^+$ extrathymic AIRE-expressing cells (eTACs—including Janus and AIRE$^+$ ILC3-like cells), as well as other surfacing populations like Thetis cells (28–31, 34, 35). Their lineage relationships and functional specializations are ill-defined because RORγt-expressing APCs phenotypically resemble each other and share expression of CD11c and ZBTB46 with cDCs (25,

[1]Present address: Immune Regulation Laboratory, Center of Basic Research, Biomedical Research Foundation Academy of Athens, 11527 Athens, Greece.

[2]Present address: Helmholtz Centre for Infection Research, Braunschweig 38124, Germany.

[3]To whom correspondence may be addressed. Email: Barbara.schraml@bmc.med.lmu.de.

This article contains supporting information online at https://www.pnas.org/lookup/suppl/doi:10.1073/pnas.2417308122/-/DCSupplemental.

Published February 24, 2025.

29, 30, 35, 36). Janus cells express *Aire*, RORγt and the integrin b8 (*Itgb8*) but lack ILC3 markers CXCR6 and IL7R. They phenotypically and transcriptionally resemble CCR7$^+$ migratory cDCs (29, 35) and have primarily been profiled from pooled cervical, brachial, axillary, inguinal, and mesenteric lymph nodes (mLN) (35). Thus, it is unclear if they exhibit site-specific heterogeneity. Thetis cells have first been described in neonatal mLN and resemble Janus cells although they are apparently absent from skin draining LN (30). Only a fraction of Thetis cells (TCI and TCIII) expresses *Aire*, while TCIV expresses *Itgb8* but lacks *Aire* (30). While Janus and Thetis cells in mice drive T cell tolerance, human R-DC-like cells that resemble Thetis cells can activate allogeneic T cells (37). Thus, the above cell types may function beyond T cell tolerance, highlighting the need for a more accurate alignment of Janus cells, Thetis cells, and RORγt$^+$ eTAC subsets, and the tissue-specific signals that regulate them.

cDC2B from adult mouse spleen show accessible chromatin at ROR response elements (RORE) in bulk ATAC sequencing, leading to the notion that cDC2B expresses RORγt (12, 31). However, active RORγt protein expression in cDC2B from adult mice has not been reported and only a minor fraction of cDC2B show RORγt expression history (10, 12). In contrast, we have demonstrated active RORγt protein expression in a fraction of cDC2-like cells in neonatal mouse spleen and Peyer's patches, that phenotypically and transcriptionally more closely resemble cDC2A than cDC2B (10, 38). These RORγt$^+$ cDC2-like cells in the neonatal spleen do not arise from *Clec9a*-expressing myeloid cDC progenitors (10), suggesting they could be a unique type of APC, possibly related to Thetis cell subsets, which resemble cDC2 in terms of CD11b expression (30).

Here, we show that RORγt$^+$ DCs are a transcriptionally distinct and evolutionarily conserved DC subtype that reconciles various previously described RORγt$^+$ APC populations, including RORγt$^+$ eTACs, Janus and Thetis cells, RORγt$^+$ cDC2-like cells, R-DC like cells, ACY3$^+$ DCs (39) and PRDM16$^+$ cDC2C (40). We demonstrate that RORγt$^+$ DCs are ontogenetically and transcriptionally distinct from other cDC subtypes, as well as from ILC3. Yet, RORγt$^+$ DCs bear hallmark features of cDCs, including migration to lymph nodes and ability to activate naïve CD4$^+$ T cells in response to inflammatory stimuli that warrant their affiliation with DCs.

Results

RORγt$^+$ DCs Exist in the Murine Spleen Across Age. We first profiled spleens from *RORγt^{GFP}Clec9a^{Cre}Rosa^{Tom}* and *Clec9a^{Cre}Rosa^{Tom}* mice systematically across age by flow cytometry. In these mice, Tomato expression tracks cells arising from committed *Clec9*a-expressing myeloid cDC progenitors (41), while GFP expression reports the RORγt-specific isoform encoded by *Rorc* (42). We first identified MHCII$^+$ILC3s as CD90$^+$CD127$^+$MHCII$^+$GFP$^+$ cells and then gated cDCs as CD11c$^+$MHCII$^+$ cells lacking the canonical ILC3 markers CD90 and CD127—also known as interleukin-7 receptor (IL-7R) (Fig. 1*A* and *SI Appendix*, Fig. S1*A*). Within CD11c$^+$MHCII$^+$ splenocytes, we detected GFP-expressing cells at all ages examined (Fig. 1*A*). Importantly, GFP$^+$CD11c$^+$MHCII$^+$ cells also stained with an anti-RORC antibody (Fig. 1*E*), confirming that GFP signal in *RORγt^{GFP}* mice accurately reports RORγt protein expression and that anti-RORC antibody staining in CD11c$^+$MHCII$^+$ cells predominantly identifies cells expressing the γt isoform of RORC. Unbiased gating of GFP$^+$ cells showed that RORγt$^+$CD11c$^+$MHCII$^+$ cells lacked ILC3 markers CD127, CD90, and CXCR6 (Fig. 1 *B* and *C* and *SI Appendix*, Fig. S1 *B* and *C*). The frequency of RORγt$^+$ cells within CD11c$^+$MHCII$^+$ cells declined with age; however, their absolute numbers correlated with organ size and increased until weaning age and remained constant until adulthood (8 to 15 wk of age, Fig. 1*F* and *SI Appendix*, Fig. S1*D*).

We had previously found that CD11b$^+$ RORγt$^+$ cDC2-like cells were nearly undetectable by two weeks of age (10). Indeed, at one week of age, CD11c$^+$MHCII$^+$RORγt$^+$ cells uniformly expressed CD11b but lacked CD24. Starting at two weeks of age RORγt$^+$ cells showed a CD11b^{low} to negative phenotype, while retaining the cDC2 marker CD172a (10) (Fig. 1*D*), and stained positive for CD24 (Fig. 1 *A* and *B*). At all ages examined RORγt$^+$CD11c$^+$MHCII$^+$ cells stained negative for the cDC1-specific marker XCR1 (Fig. 1*B*). Thus, the apparent lack of CD11b by two weeks of age explains why we had previously missed these cells in adult mice and suggests that these cells are either heterogenous or change their phenotype with age. In line with our previous work (10), RORγt$^+$CD11c$^+$MHCII$^+$ cells lacked Tomato expression in *Clec9a^{Cre}Rosa^{TOM}* mice at all ages examined, supporting that they do not arise from *Clec9a*-expressing DC progenitors (10, 41). RORγt$^+$CD11c$^+$MHCII$^+$ cells were present in *Rag2$^{-/-}$γc$^{-/-}$* mice, which lack lymphocytes, including ILC3s and their precursors (Fig. 1 *G* and *H*) (43), but fate mapped prominently in lymphoid-specific hCD2^{iCre}Rosa^{YFP} lineage-tracer mice (*SI Appendix*, Fig. S1*E*). RORγt$^+$CD11c$^+$MHCII$^+$ cells were strongly reduced in mice deficient for fms-like tyrosine kinase 3 ligand (FLT3L) (Fig. 1*I*), a growth factor critical for the development of all DCs and ILCs (44, 45). Thus, RORγt$^+$CD11c$^+$MHCII$^+$ cells exist in the murine spleen across age and can either be detected using an anti-RORC antibody or by GFP signal in *RORγt^{GFP}* mice (Fig. 1 *A* and *E*). As these cells do not develop in FLT3L$^{-/-}$ mice and phenotypically resemble DCs (10), we refer to these cells as RORγt$^+$ DCs from hereon in accordance with suggestions for DC and ILC nomenclature (1, 31, 46).

Single-Cell Multiomic Profiling Aligns Murine RORγt$^+$ DCs with Janus Cells, RORγt$^+$ eTACs and Thetis Cells. To gain insight into the transcriptional and regulatory relatedness of RORγt$^+$ DCs to cDCs and ILC3s across age, we performed paired single-cell RNA sequencing (scRNA-seq) and single-cell assay for transposase-accessible chromatin (scATAC) from the same cell using 10X multiomic profiling. RORγt$^+$ DCs and MHCII$^+$ILC3s were sorted from spleens of two-week-old or adult *RORγt^{GFP}* mice and mixed at a 1:1 ratio to enrich for RORγt$^+$ DCs. CD11c$^+$MHCII$^+$ cDCs were added in 10-fold excess to capture their heterogeneity. After quality filtering, we retained chromatin accessibility and gene expression profiles from 9,899 and 11,980 nuclei respectively. Unsupervised clustering based on gene expression (RNA) and open chromatin (ATAC) profiles revealed 18 and 16 clusters, respectively, that were largely congruent and could be classified as cDC1, cDC2, migratory cDCs (migDCs), ILC3s, pDCs, and tDCs (Fig. 2*A* and *SI Appendix*, Fig. S2 *A–F* and Table S1). cDC2 split into 5 clusters based on gene expression, of which clusters 1, 2, and 3 corresponded to cDC2A (12, 47) (*SI Appendix*, Fig. S2*C*). Of note, cDC2 clusters 1 and 2 showed uniform chromatin accessibility (*SI Appendix*, Fig. S2 *B* and *D*), as discussed below. cDC2 clusters 4 and 5 transcriptionally resembled both cDC2B and DC3 and were denoted as cDC2B/DC3 as they could not confidently be delineated as either cell type (Fig. 2*A* and *SI Appendix*, Fig. S2 *C* and *E*) (11, 12). pDCs showed uniform chromatin accessibility but split into two clusters based on gene expression (*SI Appendix*, Fig. S2 *A*, *B*, and *D*). *Rorc*$^+$ cells distributed across 5 clusters, of which ILC3_1 and ILC3_2 scored high for ILC3 signature genes and expressed *Rora, Il7r, Cxcr6*, and one cluster transcriptionally resembled ex-ILC3 (48) (Fig. 2 *A* and *B* and *SI Appendix*, Fig. S2*C* and Table S2). Additionally, one cluster expressed *Rorc*, *Prdm16,* and *Lingo4* (10) while lacking *Il7r, Rora*, and *Cxcr6* and transcriptionally resembled RORγt$^+$ cDC2-like cells from neonatal

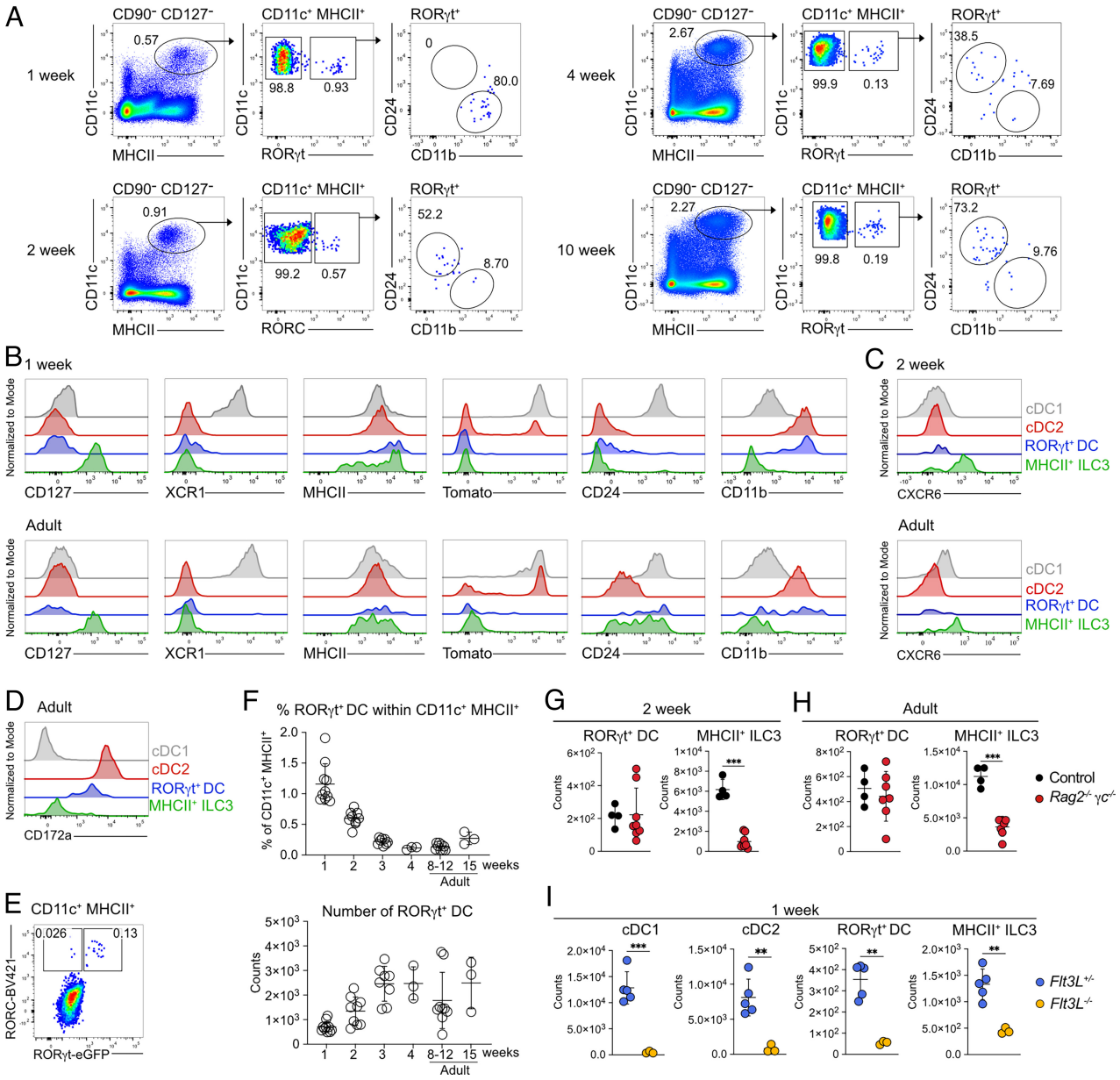

Fig. 1. RORγt$^+$ DCs exist in the murine spleen across age. (*A* and *B*) Splenocytes from *Clec9a*^{Cre}*Rosa*^{Tom} or *Clec9a*^{Cre}*Rosa*^{Tom}*RORγt*^{GFP} mice at the indicated ages were analyzed by flow cytometry. (*A*) Live CD90$^-$CD127$^-$CD11c$^+$MHCII$^+$ cells were gated and RORγt$^+$ cells revealed by GFP or anti-RORC intranuclear staining (2-wk time point). GFP$^+$ or RORC$^+$ cells were further analyzed for CD11b and CD24 expression. (*B–D*) Expression of the indicated surface markers in cDC1 (gray), cDC2 (red), MHCII$^+$ ILC3 (green), and CD11c$^+$MHCII$^+$RORγt$^+$ cells (blue) from spleens of mice at the indicated ages. Gating strategy *SI Appendix*, Fig. S1*A*. (*E*) CD11c$^+$MHCII$^+$ cells from *RORγt*^{GFP} mice were stained using an anti-RORC antibody to demonstrate that anti-RORC staining and RORγt driven GFP are largely congruent. (*F*) Frequency of RORγt$^+$ cells within CD11c$^+$MHCII$^+$ cells and number of RORγt$^+$ DCs in spleens of the indicated ages (1-wk-old n = 10; 2-wk-old, n = 9; 3-wk-old n = 8, 4-wk-old n = 3; 8 to 12-wk-old n = 6; 15-wk-old n = 3). Data are pooled from 1 to 2 independent experiments; each data point represents a biological replicate. (*G* and *H*) MHCII$^+$ ILC3 and RORγt$^+$ DCs were quantified in spleens from 2-wk-old (*G*) and adult *Rag2*$^{-/-}$*γc*$^{-/-}$ mice (*H*) and littermate controls. Each data point represents an individual mouse from two independent experiments. (*I*) Quantification of cDC1, cDC2, RORγt$^+$ DC, and MHCII$^+$ ILC3 in spleens from 1-wk-old *Flt3l*$^{-/-}$ and *Flt3l*$^{+/-}$ littermate controls. RORγt$^+$ DC quantified by intranuclear staining against RORC. Each dot represents one mouse, horizontal bars represent mean, error bars represent SD. ***P* (0.0021) ****P* (0.0002). Statistical analyses in (*G–I*) were performed using two-tailed Welch's *t* test.

mouse spleen (10), establishing it as RORγt$^+$ DCs (Fig. 2 *B–D* and *SI Appendix*, Table S1). This cluster expressed higher levels of *Ccr6*, *Cd200,* and *Epcam* compared to other DC subtypes and we could confirm higher expression of these markers on RORγt$^+$ DCs compared to cDC1 and cDC2 by flow cytometry (Fig. 2*F*).

Some migratory DCs expressed *Aire* (Fig. 2 *B* and *D*), as expected (35, 49) but we could also identify a distinct cluster of cells expressing *Aire, Rorc,* and *Prdm16*, which we termed RORγt$^+$ eTACs. RORγt$^+$ DCs and RORγt$^+$ eTACs most closely resembled each other and migratory cDCs transcriptionally and based on chromatin accessibility (Fig. 2*E*). While RORγt$^+$ eTACs and RORγt$^+$ DCs showed similar chromatin accessibility, they somewhat diverged based on gene expression profile (Fig. 2*A*). The *Aire* locus, including the conserved noncoding sequence 1 (CNS1) region (35) showed accessible chromatin peaks in migDCs, RORγt$^+$ DCs and RORγt$^+$ eTACs. Highest accessibility of the CNS1 region was observed in RORγt$^+$ eTACs and RORγt$^+$ DCs; however, some cell type–specific peaks were observed close to the transcriptional start site of *Aire* only in RORγt$^+$ eTACs (Fig. 2*G*). The RORγt$^+$ DC cluster was distinguished from other clusters by expression of genes including *Prdm16, Col17a1, Pigr, Ltb,* and *Lingo4*, of which *Prdm16* and *Col17a1* expression were shared with RORγt$^+$ eTACs (Fig. 2*D* and *SI Appendix*, Table S2). RORγt$^+$ eTACs showed specific expression of *Aire, Tnfrsf11a* (RANK), and *Itgb8* (Fig. 2*D*). Flow cytometry in

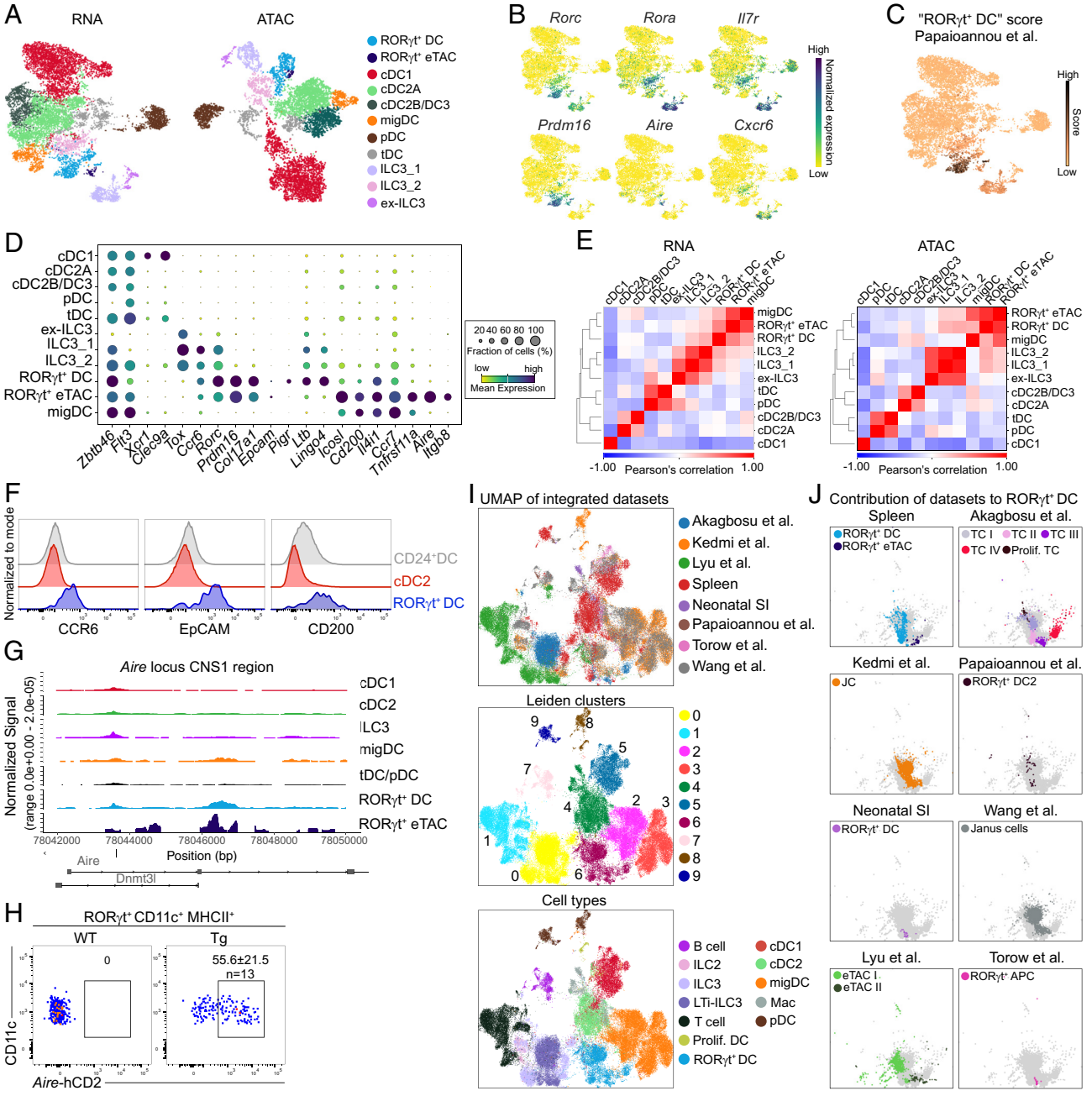

Fig. 2. Integrative transcriptional analyses align RORγt⁺ DCs with Janus cells, RORγt⁺ eTACs and Thetis cells. (*A–E*) Single-cell multiomic profiling (paired scATAC and scRNA-seq) of RORγt⁺ DCs, RORγt^{neg}CD11c⁺MHCII⁺ cells, and MHCII⁺ ILC3 from spleens of two-week-old (n = 2) or adult (n = 3) *RORγt^{GFP}* mice was performed. (*A*) RNA-based and ATAC-based UMAP of 11,980 nuclei annotated by cell type (see also *SI Appendix*, Fig. S2). (*B*) Expression of indicated genes on the RNA-based UMAP. (*C*) RNA-based UMAP depicting enrichment score for genes that distinguished RORγt⁺ cDC2-like cells in the neonatal spleen (10). (*D*) Bubble plot of select cell type defining genes. (*E*) Pearson's correlation to show the similarity between clusters identified based on RNA and ATAC profiles. (*F*) Staining of the indicated surface markers on RORγt⁺ DCs (blue), cDC2 (red), and CD24⁺ DCs (gray). (*G*) Chromatin accessibility at the CNS1 region of *Aire* locus in the indicated cell types. (*H*) AIRE expression in RORγt⁺CD11c⁺MHCII⁺ cells revealed by anti-hCD2 staining in the spleen of adult *Aire^{hCD2}* mice. (*I*) The indicated murine datasets were integrated. UMAP of the integrated datasets colored by dataset and by Leiden clusters. (*J*) Zoomed-in display of the RORγt⁺ DC cluster from the UMAP in (*I*) with all cells contributing to the cluster in gray. The contribution of the specified populations from the indicated publications is shown.

Aire^{hCD2} reporter mice (50) confirmed that a fraction of RORγt⁺ DCs indeed express AIRE (Fig. 2*H*) but *Aire* deficiency did not influence the development of RORγt⁺ DCs in mixed bone marrow chimeras (*SI Appendix*, Fig. S2*G*). AIRE⁺ RORγt⁺ DCs stained slightly higher for CCR7, CD24, MCHII, and CD200 but resembled AIRE^{neg} RORγt⁺ DCs in terms of EpCAM, ICOSL, and CCR6 expression (*SI Appendix*, Fig. S2*H*). Altogether, these data suggest that RORγt⁺ eTACs are a transcriptional state of RORγt⁺ DCs.

Some of the aforementioned genes (*Prdm16, Col17a1, Pigr, Ltb, Aire, Tnfrsf11a*) have been reported in Thetis cells and Janus cells/eTACs (29, 30, 34, 35). Therefore, we performed data integration of the above dataset, together with published scRNA-seq datasets of DCs from neonatal murine spleen (10), RORγt⁺ APCs from neonatal Peyer's patch (38), Thetis cells from neonatal mLN (30), Janus cells from mLN (*SI Appendix*, Fig. S3 *C* and *D*) and sdLN (29, 35), and RORγt⁺ eTACs from mLN (23). We additionally integrated scRNA-seq data from neonatal small intestine in which we identified a cluster of RORγt-expressing DCs (*SI Appendix*, Fig. S3 *A* and *B*). After unsupervised dataset integration using scVI (51) cells from individual datasets were distributed evenly across

Leiden clusters (Fig. 2*I*). Cells originally annotated as the same broad cell types in the individual datasets (cDC1, cDC2, migDCs, pDCs, ILC3) clustered together in the integrated analysis irrespective of study and tissue of origin, and Leiden clusters corresponded well to the different cell types included (Fig. 2*I* and *SI Appendix*, Fig. S2*I*). We found that cells originally annotated as eTACs, Janus cells, Thetis cells, or RORγt$^+$ APCs clustered together with RORγt$^+$ DCs identified in our study, into a transcriptionally distinct cluster (Leiden 6), termed RORγt$^+$ DCs (Fig. 2*J* and *SI Appendix*, Fig. S2*I*). Of note, Thetis cells from neonatal mLN also show heterogeneity in terms of *Aire* expression (*SI Appendix*, Fig. S2*J*) (30), supporting that RORγt$^+$ DCs entail distinct transcriptional states. Together, this comprehensive multiomic profiling and meta-analysis establishes RORγt$^+$ DCs as a transcriptionally distinct cell type with strong resemblance to RORγt$^+$ eTACs, Janus and Thetis cells.

Comparative Transcriptomics Reveals RORγt$^+$ DCs are Evolutionarily Conserved. To investigate whether RORγt$^+$ DCs exist in the human spleen, we analyzed a scRNA-seq dataset of human spleen cDCs from a 61-year-old patient (12). 11 of 12 identified clusters corresponded to the previously identified clusters, including cDC1, CLEC10A$^-$ cDC2A, and CLEC10A$^+$ cDC2B, DC progenitor-like cells (pre-DC/ASDCs), CCR7$^+$ migratory DCs (CCR7$^+$ DCs), and one cluster of dividing cells (Fig. 3*A* and *SI Appendix*, Fig. S4 *A–C*). Cluster 11 expressed *RORC* and *PRDM16,* but not the ILC3 genes *RORA* and *IL7R* (*SI Appendix*, Fig. S4*C*), and had been excluded from the original analyses as putative ILC3 contamination. Indeed, this *RORC*$^+$ cluster scored high for expression of ILC3 signature genes (Fig. 3*B*) but also for genes that distinguished RORγt$^+$ DCs in multiome and scRNA-seq analyses from murine spleen (10) (Fig. 3*B* and *SI Appendix*, Table S1). From the Tabula Sapiens human reference atlas, we selected spleen cells annotated as CD1c$^+$ and CD141$^+$ myeloid DCs, pDCs, and ILCs (52), which formed 8 clusters corresponding to cDC1 (cluster 2), cDC2 (cluster 4), ILC3 (cluster 1, 0, 5), and pDCs (clusters 6 and 3) (Fig. 3 *C* and *D* and *SI Appendix*, Fig. S4 *D–F*). Cells in cluster 7 expressed *RORC* and *PRDM16,* but not *RORA* and *IL7R* and scored highest for genes distinguishing RORγt$^+$ DCs in mouse spleen, whereas ILC3s scored highest for ILC3 signature genes (Fig. 3*D* and *SI Appendix*, Table S1). This *RORC*$^+$ cluster contained cells from multiple donors aged 59, 61, and 69 y and did not segregate by the sequencing method or cell cycle phase, validating it as a bona fide population (*SI Appendix*, Fig. S4*F*). After integration, *RORC*$^+$ cells from both datasets clustered together and away from DCs and ILCs (Fig. 3 *E* and *F*). Comparative gene expression analyses identified conserved markers, including *PRDM16, UBE2E2, IL4I1, PIGR,* and *LTB,* that distinguished RORγt$^+$ DCs in murine spleen and the *RORC*$^+$ clusters in the human spleen (Fig. 3*G*). Thus, RORγt$^+$ DCs also exist in the human spleen.

We also identified *RORC*- and *PRDM16*-expressing cells that lacked *RORA* and resembled the *RORC*$^+$ cluster in the human spleen in single-cell RNA-seq data from small and large intestines from healthy adults (25 to 75 y old) (53) (*SI Appendix*, Fig. S5 *A–D* and Table S5), as well as in small intestine of healthy pediatric donors and pediatric Crohn's disease patients (*SI Appendix*, Fig. S5*E*). These data indicate that RORγt$^+$ DCs are conserved in the human intestine across age. In the Tabula Sapiens lymph node dataset (52), we also detected *RORC*-, *PRDM16*-, and *LTB*-expressing cells, some of which expressed *AIRE* (*SI Appendix*, Fig. S5 *F–I*), and that derived from multiple donors and anatomically distinct LNs (*SI Appendix*, Fig. S5 *F* and *H*) and have recently been dubbed cDC2C (40).

By performing comparative gene expression analyses of RORγt$^+$ DCs in each dataset described above and identifying commonalities, we revealed a set of genes, including *RORC*, *PRDM16*, *LTB*, *PIGR*, and *IL4I1,* that reliably distinguished RORγt$^+$ DCs across tissues and species in all of the above mouse and human datasets (Fig. 3 *H* and *I* and *SI Appendix*, Tables S1 and S5 and Fig. S6 *E* and *F*). R-DC-like cells from tonsil, which correspond to Thetis cells (37) showed higher expression of these genes compared to other populations in the same dataset (Fig. 3*H*), indicating that these cells are homologous to RORγt$^+$ DCs. Additionally, we could align RORγt$^+$ DCs with PRDM16$^+$ cDC2C from glioblastoma (GBM) (40, 54) and ACY3$^+$ DCs from cerebral spinal fluid (CSF) of patients with multiple sclerosis (39) (Fig. 3*H* and *SI Appendix*, Fig. S6 *A* and *B*) and identified RORγt$^+$ DCs in two additional datasets from CSF of patients with demyelinating disease (55, 56) (*SI Appendix*, Fig. S6 *C–E*). This comprehensive meta-analysis establishes RORγt$^+$ DCs as a transcriptionally distinct and evolutionarily conserved cell type that encompasses previously described populations including RORγt$^+$ eTACs, Janus cells, Thetis cells, R-DC-like cells, cDC2C and ACY3$^+$ DCs.

Distribution and Phenotype of RORγt$^+$ DCs Across Lymphoid and Nonlymphoid Tissues in Mice. We next assessed the tissue distribution of RORγt$^+$ DCs across age in *RORγt*^{GFP} mice. Migratory cDCs in nonlymphoid tissues express CD127 (25, 57) (*SI Appendix*, Fig. S7*A*). Thus, we gated cDCs irrespective of CD127 as CD90$^-$ CD11c$^+$MHCII$^+$ cells negative for the monocyte marker CD64. In mLN, we detected RORγt$^+$ DCs at all ages examined and found their frequency was highest in neonatal mLN and declined with age (Fig. 4*A*). As reported (30), we consistently detected the highest numbers of RORγt$^+$ DCs at two weeks of age (Fig. 4*A* and *SI Appendix*, Fig. S7*B*). In small intestinal lamina propria (siLP) the frequency of RORγt$^+$ DCs within CD11c$^+$MHCII$^+$ cDCs was highest in neonates and absolute numbers peaked at two weeks of age (Fig. 4*B*). Of note, for technical reasons, Peyer's patches (PP) were removed from SI only for mice older than two weeks (Fig. 4*B*). RORγt$^+$ DCs were present in the colon, which lacks PP, of neonatal and adult mice (Fig. 4*C*). RORγt$^+$ DCs differed phenotypically from MHCII$^+$ILC3s (CD90$^+$CD127$^+$MHCII$^+$GFP$^+$ cells, *SI Appendix*, Fig. S7 *A*, *C*, *E*, and *F*) and in mLN lacked the ILC3 marker CXCR6 (*SI Appendix*, Fig. S7*D*). In mLN and siLP from one-week-old, but not adult mice, RORγt$^+$ DCs expressed CD11b (*SI Appendix*, Fig. S7 *C* and *F*). In both tissues RORγt$^+$ DCs expressed high levels of MHCII, consistent with a migratory DC phenotype and lacked the cDC1 marker XCR1, although some RORγt$^+$ DCs expressed XCR1 in adult mLN (*SI Appendix*, Fig. S7 *C* and *F*). In the lung, RORγt$^+$ DCs were least frequent and their numbers peaked at two weeks of age (Fig. 4*D* and *SI Appendix*, Fig. S8 *A–C*). Pulmonary RORγt$^+$ DCs lacked XCR1 but expressed CD11b and were distinguished from ILC3s by expression of CD11c, MHCII and lack of CD90 (*SI Appendix*, Fig. S8 *A* and *B*). Importantly, we also detected RORγt$^+$ DCs with high MHCII expression in skin draining lymph nodes (Fig. 4*E* and *SI Appendix*, Fig. S8 *D–F*).

Transcriptional Regulation of RORγt$^+$ DCs. We next investigated the transcriptional regulation of RORγt$^+$ DCs in the spleen (Fig. 2). While cells from different ages distributed evenly across ATAC and RNA clusters, RNA cluster cDC2_2 was dominated by cells from the adult time point (*SI Appendix*, Fig. S9*A*). Because cDC2 clusters 1 and 2 showed uniform chromatin accessibility but split into two clusters based on gene expression (*SI Appendix*, Fig. S2 *A*, *B*, and *D*), these data indicate that while cDC2 chromatin identity is conserved environmental signals may shape gene expression in cDC2 across age, as reported (10, 38, 58). Accordingly, we identified 687 differentially expressed genes between the cDC2 metacluster across age (*SI Appendix*, Table S3). cDC2 from adult mice were enriched for genes downstream of IFNγ, tumor

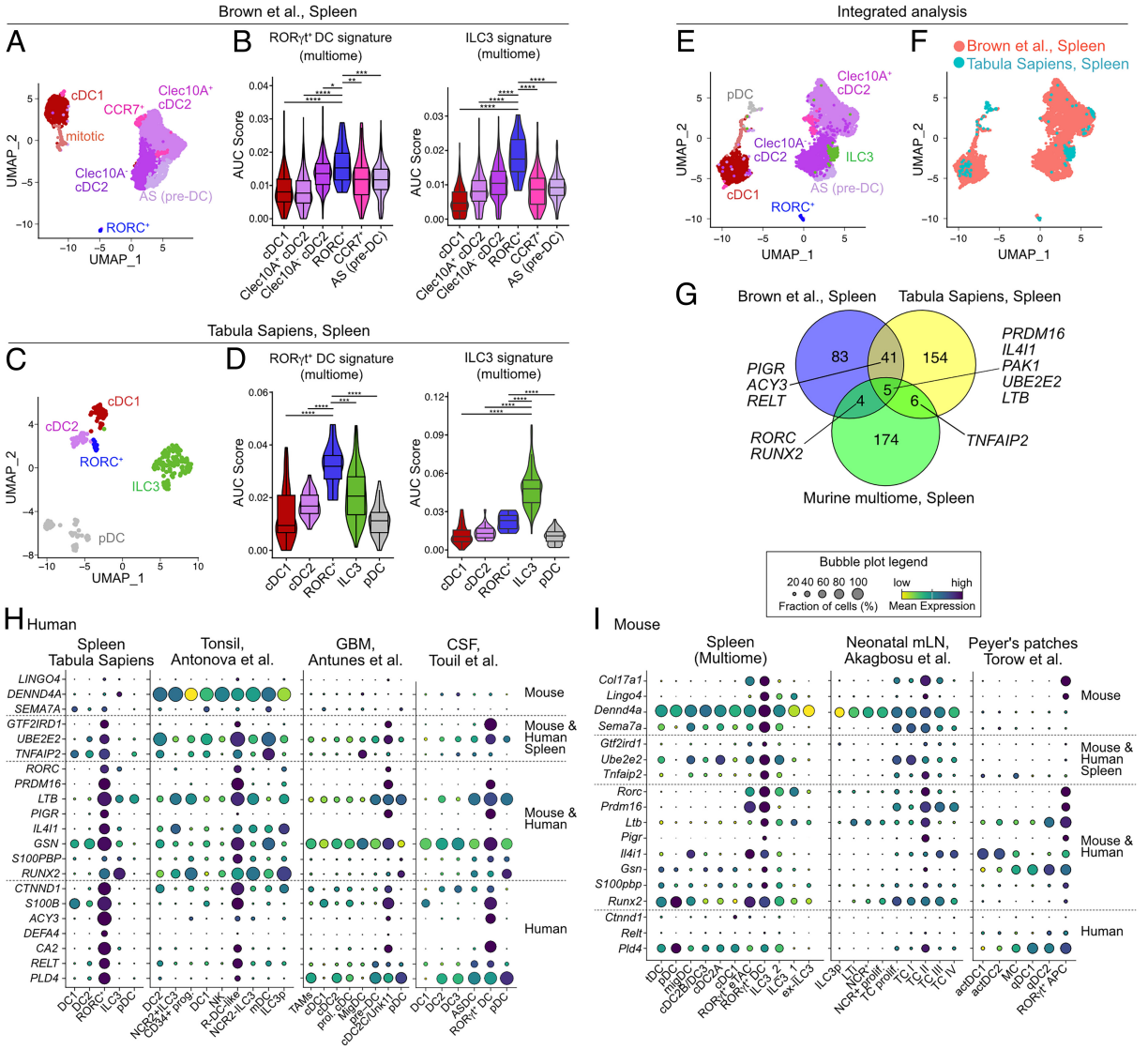

Fig. 3. Comparative transcriptomics reveals RORγt$^+$ DCs are evolutionarily conserved. (*A*) Annotated UMAP of 4,717 cells from scRNA-seq dataset of human splenic DCs. (*B*) Enrichment scores for the RORγt$^+$ DC and ILC3 signatures from the murine multiome dataset were calculated for each cluster. (*C*) Annotated UMAP of 262 cells from scRNA-seq dataset of human spleen. (*D*) Enrichment scores for the RORγt$^+$ DC signature or ILC3 signature from the murine multiome dataset were calculated for each cluster. (*E* and *F*) Annotated UMAP (*E*) of integrated scRNA-seq datasets generated using Seurat Integration of scRNA-seq datasets pipeline, and colored by dataset (*F*). (*G*) Venn diagram showing the overlap of genes distinguishing RORγt$^+$ DCs in the indicated mouse and human scRNA-seq datasets. (*H* and *I*) Bubble plots of selected genes deduced from comparative gene expression analyses that distinguish RORγt$^+$ DCs in various human (*H*) and murine (*I*) scRNA-seq datasets. Genes are ordered according to the species and organs they were found in to differentiate RORγt$^+$ DCs from other cell types. *P < 0.05, **P < 0.01, ***P < 0.001, ****P < 0.0001. Statistical analysis was performed using the Wilcoxon nonparametric ranked sum test.

necrosis factor-α (TNF-α), IL-2, and IFNα signaling (*SI Appendix*, Fig. S9*B*), corroborating our previous findings (10), and validating the suitability of our dataset to compare populations across age. Contrary to cDC2, RORγt$^+$ DC clusters had equal contribution of cells from both ages and only 29 genes were differentially expressed between RORγt$^+$ DCs across age (*SI Appendix*, Fig. S9*A* and Table S3). Thus, RORγt$^+$ DCs are transcriptionally stable between 2 wk of age and adulthood.

Focused multiomic analysis of the RORγt$^+$ DC and RORγt$^+$ eTAC clusters confirmed that RORγt$^+$ eTACs form a separate cluster from RORγt$^+$ DCs in ATAC and mRNA profiles (Fig. 5 *A* and *B* and *SI Appendix*, Fig. S9*C*). *Aire*^{neg}RORγt$^+$ DCs could further be divided into 3 clusters (Fig. 5 *A* and *B* and *SI Appendix*, Fig. S9*C*). Of note, *Itgb8* expression, which promotes Treg differentiation (29, 30) was restricted to the RORγt$^+$ eTAC cluster (Fig. 5*B*). RORγt$^+$ DC cluster b showed lower expression of *Rorc* than the other two clusters (Fig. 5*B*), suggesting that RORγt$^+$ DCs can lose RORγt expression. Indeed, in spleens from two-week-old and adult *RORγt*^{Cre}*Rosa*^{YFP}*RORγt*$^{GFP\text{-}knockin}$ reporter mice cells with RORγt expression history (YFP) outnumbered those with active RORγt expression (GFP; Fig. 5*C*) although these cells were otherwise phenotypically similar (*SI Appendix*, Fig. S9*D*). Similar observations were made in the lung, mLN and siLP (Fig. 5*D* and *SI Appendix*, Fig. S9*E*). Especially in lung and mLN from two-week-old mice, cells with *RORγt*^{Cre} expression history largely outnumbered those actively expressing RORγt (Fig. 5*D* and *SI Appendix*, Fig. S9*E*).

Finally, combining chromatin accessibility and gene expression profiles from individual cells we used SCENIC+ (59) to identify cell type–specific enhancer-driven gene regulatory networks (eRegulons). Dimensionality reduction based on target gene and target region enrichment scores of eRegulons separated the same main cell states as identified above (Fig. 5*E*). Of note, RORγt$^+$ DCs and RORγt$^+$ eTACs were similar in this analysis suggesting that they are closely related cell states. SCENIC+ identified well-known master regulators of cDC1 (*Irf8*), cDC2 (*Runx3*), pDCs (*Tcf4/E2-2, Spib*), and ILC3 (*Rora, Ikzf1, Rorc*), confirming the

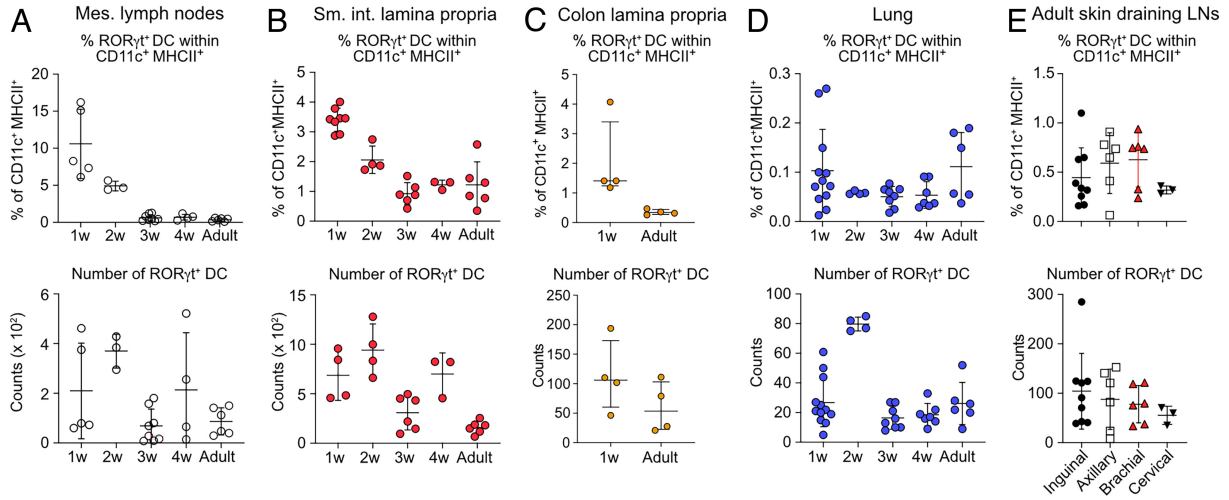

Fig. 4. RORγt$^+$ DCs exist across lymphoid and nonlymphoid tissues in mice and humans. (*A–C*) RORγt$^+$ DCs were quantified in mLN (*A*), siLP (*B*) colon LP (*C*), lung (*D*), and skin draining lymph nodes (*E*) of *RORγt^{GFP}* reporter mice (representative gating in *SI Appendix*, Fig. S7 and S8). (*A*) Frequency of RORγt$^+$ cells within CD11c$^+$MHCII$^+$ cells (*Upper* plot) and number of RORγt$^+$ cells (*Lower* plot) in mLN of mice of indicated ages (1 wk n = 5; 2 wk n = 3; 3 wk n = 8, 4 wk n = 4; Adult n = 6). (*B–D*) Frequency of RORγt$^+$ cells within CD11c$^+$MHCII$^+$CD64$^-$ cells (*Top*) and number (*Bottom*) in siLP (1-wk-old n = 4 to 8; 2-wk-old n = 4; 3-wk-old n = 6, 4-wk-old n = 3; Adult n = 6), colon (1-wk-old n = 4; adult n = 4), and lung (1-wk-old n = 11; 2-wk-old n = 4; 3-wk-old n = 7, 4-wk-old n = 6; Adult n = 6) from mice of indicated ages. (*E*) RORγt$^+$ DCs from axial, brachial, cervical, and inguinal skin draining LN were gated as in *SI Appendix*, Fig. S8*D* and quantified. The frequency of RORγt$^+$ cells within CD11c$^+$MHCII$^+$ cells (*Top*) and number of RORγt$^+$ DCs (*Bottom*) is shown.

validity of our approach (*SI Appendix*, Fig. S9*F*). RORγt$^+$ DCs and RORγt$^+$ eTACS shared regulatory networks *Nfat5* and *Relb* with migDCs and *Rel* with cDC2 and migDCs, aligning them with DCs (Fig. 5*F* and *SI Appendix*, Fig. S9*F*). SCENIC+ predicted RORγt$^+$ DCs and RORγt$^+$ eTACs to be specifically regulated by *Prdm16*, which is also specifically expressed in these cells (Figs. 2 *B* and *D* and 5*F* and *SI Appendix*, Fig. S9*F*). eRegulons of the nuclear receptors *Thrb/Nr1a2, Rorc,* and *Ppara* were equally predicted by SCENIC+ to regulate RORγt$^+$ DCs (Fig. 5*G* and *SI Appendix*, Fig. S9*F*). PRDM16 is a master regulator of brown adipogenesis that in adipocytes directly controls expression of *Ppara*, a nuclear receptor that, like RORγt, integrates signals from free fatty acids and is involved in lipid metabolism (60, 61). Visualization of the eRegulons formed by *Rorc* and *Prdm16* in RORγt$^+$ DCs suggests cooperativity between these factors in RORγt$^+$ DCs (Fig. 5*G*). Downstream target genes of PRDM16 showed higher expression in RORγt$^+$ DCs and RORγt$^+$ eTACs than in other cell types and some of these genes, including *Ltb,* appear coregulated by *Prdm16* and *Rorc* (*SI Appendix*, Fig. S10*B*). SCENIC+ predicted *Rorc* to regulate expression of *Pigr*, *Gtf2ird1,* and *Col17a1* (Fig. 5*G* and *SI Appendix*, Fig. S10*B*), suggesting that RORγt shapes the identity of RORγt$^+$ DCs (Fig. 5*G*). *Prdm16* was predicted to regulate expression of *Tlr12* and *Il23a*, which showed highest expression in RORγt$^+$ DCs over other clusters (Fig. 5*G* and *SI Appendix*, Fig. S10*B*). RORγt$^+$ DCs did not show enrichment of genes reported to promote Tregs in Thetis cells (*SI Appendix*, Fig. S10*A*) (30), except for expression of *Itgb8* in a subset of RORγt$^+$ DCs expressing *Aire*. Importantly, RORγt$^+$ DCs showed comparable expression of genes involved in antigen processing and presentation to cDCs and migratory DCs (*SI Appendix*, Fig. S10*C*) and flow cytometry confirmed that RORγt$^+$ DCs express costimulatory molecules, including CD80, CD86, PD-L1, and CD83. Notably, RORγt$^+$ DCs expressed highest levels of CD40 and CCR7 when compared to cDC1 and cDC2 (*SI Appendix*, Fig. S10*D*), altogether suggesting that RORγt$^+$ DCs have the necessary machinery to serve as APCs.

RORγt$^+$ DCs are Bona Fide DCs. The capacity to activate naïve T cells is a hallmark feature of cDCs (2). We, thus, sort-purified RORγt$^+$ DCs from spleens of two-week-old and adult *RORγt^{GFP}* mice, pulsed them with Ovalbumin peptide 323 to 339 ($OVA_{323-339}$) and cultured them with cell trace violet (CTV)-labeled naïve OTII transgenic T cells from adult mice with or without T cell polarizing cytokines. cDC2 and MHCII$^+$ILC3 from the same mice were used as controls (*SI Appendix*, Fig. S11*A*). As expected, cDC2 from two-week-old and adult mice induced T cell proliferation under all conditions tested, while MHCII$^+$ILC3s were poor inducers of OTII proliferation (Fig. 6 *A* and *E* and *SI Appendix*, Fig. S11 *C, D, F,* and *G*). Under all conditions tested RORγt$^+$ DCs from two-week-old and adult mice stimulated the proliferation of naïve T cells, although to a lower extent than cDC2, and supported the differentiation of OTII cells into effector T cells, as measured by intracellular cytokine and FOXP3 staining (Fig. 6 *A–H*). While RORγt$^+$ DCs supported the differentiation of FOXP3$^+$ Tregs equally or better than cDC2, the induction of Th17 cells by RORγt$^+$ DCs was reduced compared to cDC2 (Fig. 6 *C*, *D*, *G*, and *H*). Thus, RORγt$^+$ DCs can activate naïve CD4$^+$ T cells and induce their effector differentiation with qualitative and quantitative differences compared to cDC2. In contrast, MHCII$^+$ ILC3 induced little if any T cell proliferation and may require cytokine stimulation to achieve their full APC potential (62).

We next asked whether RORγt$^+$ DCs have the capacity to process and present antigen. Specific expression of CLEC4A4 on cDC2 and RORγt$^+$ DCs from neonatal and adult mice (10), but not on cDC1 or MHCII$^+$ ILC3 (Fig. 6*I*) (63), suggested that anti-CLEC4A4-OVA (63) may allow to deliver antigen to RORγt$^+$ DCs in vivo. We thus injected adult *RORγt^{GFP}* mice with anti-CLEC4A4-OVA or isotype-matched control antibody in the presence of the adjuvant CpG-B (Fig. 6 *J–L*), which did not alter the activation status of RORγt$^+$ DCs relative to cDC1 or cDC2 (Fig. 6*M* and *SI Appendix*, Fig. S11*H*). 12 h later, we sorted 300 cDC1, cDC2, RORγt$^+$ DCs and MHCII$^+$ILC3s and cocultured them with 3000 naïve CTV-labeled OTII T cells (Fig. 6 *K* and *L*). cDC2 and RORγt$^+$ DCs induced OTII proliferation after targeting with anti-CLEC4A4-OVA but not isotype-matched control antibody (Fig. 2 *K* and *L*), demonstrating successful targeting. In contrast, cDC1 and MHCII$^+$ ILC3s did not induce T cell proliferation demonstrating cell type–specific antigen targeting (Fig. 2 *K* and *L*). OTII proliferation induced by RORγt$^+$ DCs appeared marginally lower than that achieved by cDC2, which could be due to differences in CLEC4A4 targeting efficiency, responsiveness to CpG-B,

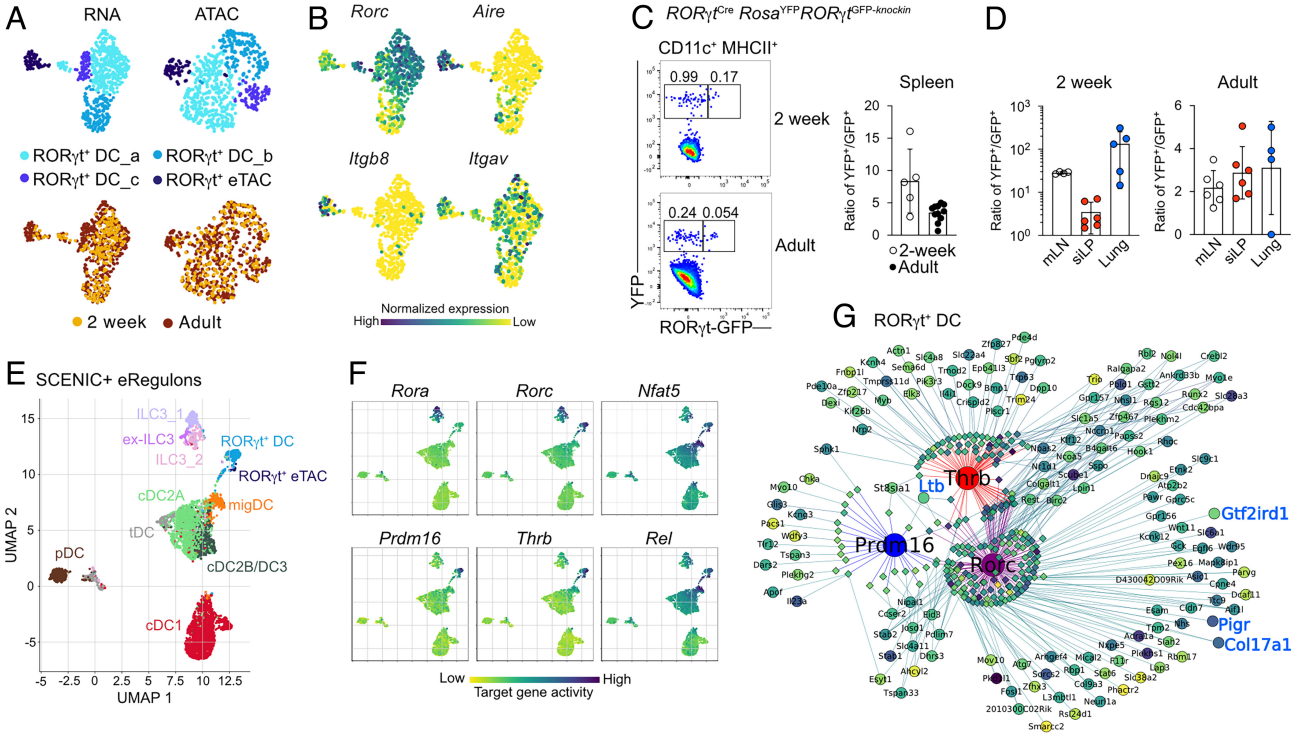

Fig. 5. Single-cell multiomic profiling reveals the unique identity of RORγt$^+$ DCs. (*A*) RORγt$^+$ DCs and RORγt$^+$ eTACs from the multiome analysis in Fig. 2 *A*–*E* were reclustered. The resulting UMAPs based on RNA and ATAC profiles are shown and annotated by timepoint. (*B*) Expression of *Rorc, Aire, Itgav,* and *Itgb8* on the RNA-based UMAP from (*A*). (*C* and *D*) Spleen (*C*), mLN, siLP and lung (*D*) from 2-week-old and adult *RORγt*^{Cre}*Rosa*^{YFP}*RORγt*$^{GFP/wt}$ mice were analyzed by flow cytometry. YFP (RORγt-expression history) versus GFP (active RORγt) expression in CD11c$^+$MHCII$^+$ cells were plotted and the ratio of YFP$^+$ to GFP$^+$ cells was calculated. Each dot represents one mouse. (*E*) UMAP display of dimensionality reduction based on target genes and region enrichment scores generated using SCENIC+. (*F*) UMAP colored by target gene activity of the indicated eRegulons predicted to regulate specific cell types (*SI Appendix*, Fig. S9*F*). (*G*) Visualization of the gene regulatory network formed by *Prdm16*, *Thrb,* and *Rorc* in RORγt$^+$ DCs. Genes that determine the identity of RORγt$^+$ DCs are colored in blue.

or expression of costimulatory molecules between RORγt$^+$ DCs and cDC2. Taken together, these data demonstrate that RORγt$^+$ DCs can process and present antigen, and activate naïve CD4$^+$ T cells in response to an inflammatory trigger.

Finally, we tested whether RORγt$^+$ DCs have the capacity to migrate to lymph nodes in response to inflammation. Gavage of neonatal mice with R848 induces cDC migration to mLN (64). Indeed, 24 h after R848 gavage we observed an increase in the frequency and number of cDC1, but not ILC3s in mLN, which served as positive and negative controls for migration, respectively (Fig. 6*N*). RORγt$^+$ DCs also increased in frequency and number in mLN (Fig. 6*N*), suggesting that oral R848 stimulates RORγt$^+$ DCs to migrate to mLN. Thus, RORγt$^+$ DCs bear classical migratory features of cDCs upon inflammatory triggers, validating their affiliation with DCs.

RORγt$^+$ DCs Exhibit a Proinflammatory Profile in Autoimmune Neuroinflammation. We next performed comparative gene expression analyses of RORγt$^+$ DCs in three independent scRNA-seq datasets from CSF of patients with autoimmune demyelinating disease and found common genes that distinguished RORγt$^+$ DCs from other cells in each dataset (Fig. 7*A*). These genes included *S100B* and *LTB*, which propagate neuroinflammation (65, 66), *TNFSF15* (TL1A), which promotes Th17 differentiation (67) and *CCR6*, which enables trafficking of DCs to LNs for the priming of autoimmune T cells in EAE (68). Of note, RORγt$^+$ DCs also expressed the aryl hydrocarbon receptor (*AHR*) and *FFAR4* (also known as GPR120), which are reported to integrate environmental signals to modulate DC function in EAE (69, 70). We thus immunized mice with MOG to induce EAE and observed an increase in frequency and number of cDC1, RORγt$^+$ DCs and MHCII$^+$ ILC3s in the brain and spinal cord of mice at peak disease compared to healthy control mice (Fig. 7 *B* and *C* and *SI Appendix*, Fig. S12*A*). Of note, in inflamed CNS, RORγt$^+$ DCs became a sizable population and reached comparable numbers to cDC1 and MHCII$^+$ ILC3s (Fig. 7 *B* and *C*), which influence EAE pathogenesis (27, 71).

Discussion

Here, we demonstrate the existence of RORγt-expressing DCs that are transcriptionally and developmentally distinct from other DC subtypes and entail murine Janus cells/ RORγt$^+$ eTACs (29, 35), Thetis cells (30), RORγt$^+$ APCs in Peyer's patches (38), as well as human R-DC-like cells (37), cDC2C (40), and ACY3$^+$ DCs (39). Previous work has demonstrated that RORγt$^+$ DCs—also known as Thetis and Janus cells induce peripheral T cell tolerance and Tregs, particularly at mucosal sites (29, 35, 72–74). We show that RORγt$^+$ DCs, like cDCs, respond to inflammation by inducing the activation of naïve T cells and that they can migrate to lymph nodes. They further accumulate in the inflamed CNS of mice and exhibit proinflammatory features in CSF of patients with inflammatory demyelinating disease, including multiple sclerosis. Thus, RORγt$^+$ DCs are bona fide immune sentinels with a versatile functional spectrum ranging from inducing T cell activation to mediating peripheral T cell tolerance (*SI Appendix*, Fig. S12*B*). This versatility makes them an attractive target for therapeutic manipulation in inflammatory diseases, cancer, and neuroinflammation.

In the spleen, RORγt$^+$ DCs lack a particular tolerogenic profile and, like cDCs, respond to inflammation with the activation of naïve CD4$^+$ T cells. Similarly, R-DC-like cells from human lymph nodes can stimulate allogeneic CD4$^+$ T cells, although their APC potential has not been compared to that of cDCs (37). Although

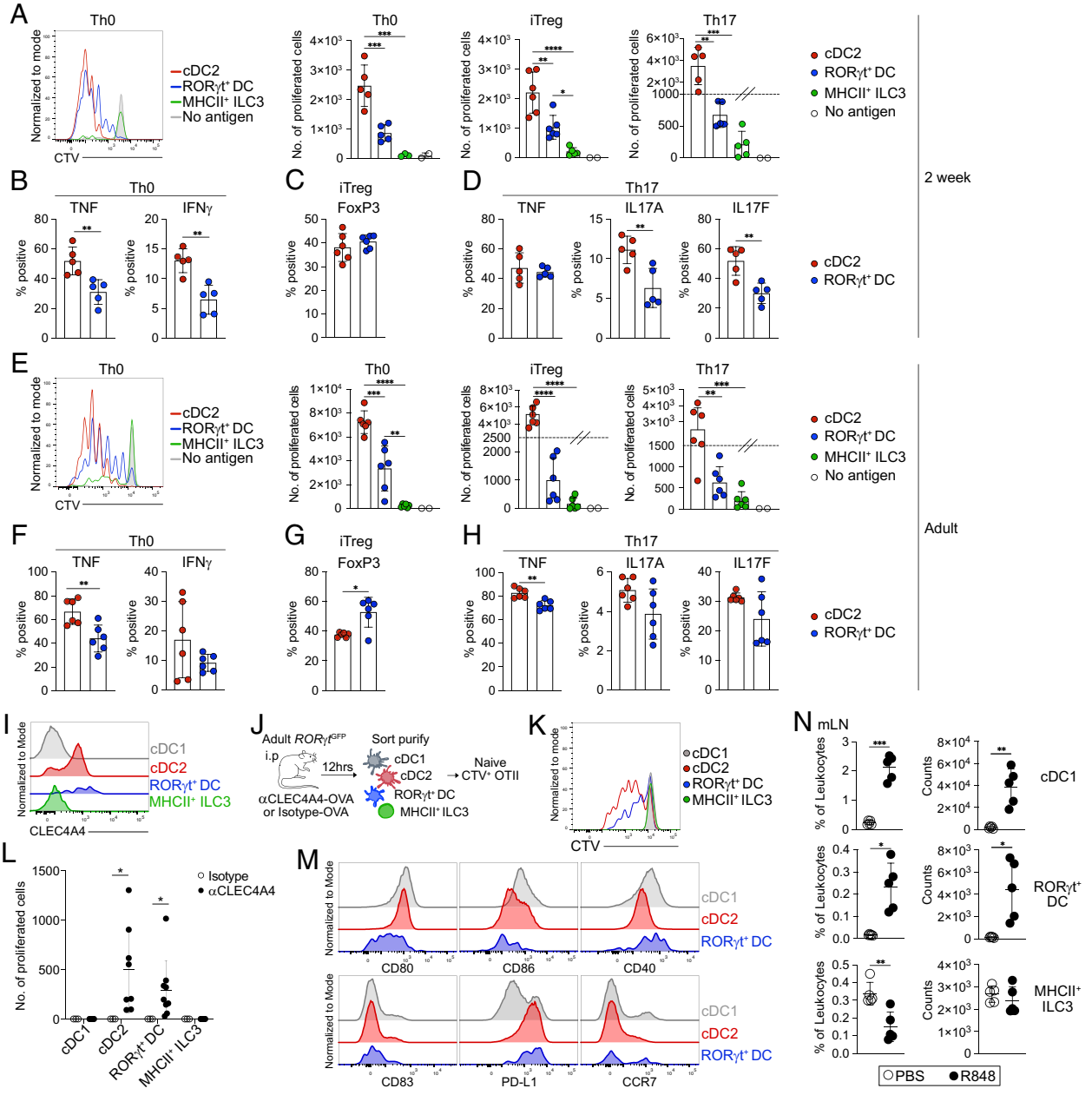

Fig. 6. RORγt$^+$ DCs are bona fide dendritic cells (DCs). (*A–H*) 250 cDC2, MHCII$^+$ ILC3, and RORγt$^+$ DCs from spleens of 2-wk-old (*A–D*) or adult (*E–H*) *RORγt^{GFP}* mice were pulsed with $OVA_{323-339}$ and cocultured with 2500 CTV-labeled naïve OTII cells as indicated. 3.5 d later, proliferation (CTV dilution), cytokine production, and FOXP3 expression in proliferated T cells were quantified. (*A*) CTV-trace of OTII cells cocultured with cDC2, RORγt$^+$ DCs, MHCII$^+$ ILC3, or cDC2 without $OVA_{323-339}$ (gray) under nonpolarizing conditions (Th0). *Right*: Quantification of proliferated cells after culture with cDC2, RORγt$^+$ DCs, MHCII$^+$ ILC3, or cDC2 without $OVA_{323-339}$ (open circle) under the indicated conditions. (*B–D*) Proliferated OTII cells were analyzed for TNF and IFNγ production (*B*), FOXP3 expression (*C*), or TNF, IL-17A, and IL-17F production (*D*). (*E–H*) OTII T cells cocultured with cDC2, MHCII$^+$ ILC3, and RORγt$^+$ DCs from adult mice were analyzed as in *A–D* above. (*I*) CLEC4A4 expression on the indicated populations. (*J–L*) Adult *RORγt^{GFP}* mice were injected i.p. with anti-CLEC4A4-OVA or isotype-OVA control antibody plus CpG-B. After 12 h 300 cDC2, cDC1, MHCII$^+$ILC3, and RORγt$^+$ DCs were sorted and cocultured with 3000 naïve CTV-labeled OTII cells. (*J*) Experimental setup. (*K*) CTV dilution and (*L*) number of proliferated OTII cells after coculture with the indicated populations (n ≥ 5). (*M*) Expression of the indicated markers on cDC1 (gray), cDC2 (red), and RORγt$^+$ DCs (blue) 12 h after i.p injection of CpG-B. (*N*) Frequency and absolute number of cDC1, MHCII$^+$ILC3, and RORγt$^+$ DCs in mLN of 11-d-old *RORγt^{GFP}* reporter mice 24 h after oral administration of R848. Each dot represents one biological replicate pooled from two independent experiments. Horizontal bars represent mean, error bars represent SD. **P* (0.0332), ***P* (0.0021) ****P* (0.0002), *****P* < 0.0001. Statistical analysis: two-tailed Welch's *t* test (*B–D*, *F–H*, and *L*) or one-way ANOVA with Tukey's multiple comparisons (*A* and *E*). Only statistically significant comparisons are indicated.

RORγt$^+$ DCs are infrequent in steady-state tissues, we found them to increase in the inflamed mLN and in the CNS of mice with active EAE. They also accumulate in the inflamed esophagus, where they express the eosinophilic esophagitis risk gene *ATP10A* (40), and in the CSF from patients with demyelinating disease (39). In patient CSF, RORγt$^+$ DCs display a proinflammatory profile and have been predicted to interact with memory CD4$^+$ T cells (39). Since RORγt$^+$ APCs contribute to CNS pathology in EAE (27), the functions of RORγt$^+$ DCs in neuroinflammation require further investigation. AhR cooperates with RORγt to drive IL-22 expression in Th17 cells (70). In patient CSF, RORγt$^+$ DCs express *AHR,* raising the possibility that these two transcription factors drive gene expression in RORγt$^+$ DCs. Since *AHR*, *FFAR4,* and *RORC* are druggable molecules, the possibility to manipulate RORγt$^+$ DCs therapeutically in EAE can be explored in future studies. The prominent expression of *LTβ* in RORγt$^+$ DCs suggest

that they can contribute to the spatial organization of immune cells (75). RORγt$^+$ DCs also express the tryptophan-metabolizing enzyme IL4i1 that generates bioactive immunomodulatory metabolites (76). IL4i1-derived metabolites can for instance activate AhR or protect cells from ferroptosis (76), suggesting that RORγt$^+$ DCs may function beyond T cell priming, for instance, by modulating metabolic communication between cells.

Taken together, the above data suggest that RORγt$^+$ DCs exhibit tissue-specific functional diversity. Tolerogenic immune functions in RORγt$^+$ APCs have been linked to AIRE (29, 35), the expression of which is restricted to subtypes of RORγt$^+$ DCs (29, 30). *AIRE* shapes gene expression in tumor-associated macrophages, DCs and ILC3s (28, 49). Our data suggest that *Aire* marks a distinct functional state since AIRE$^+$RORγt$^+$ DCs express higher levels of CCR7 and MHCII than AIRE^{neg} cells and show a distinct transcriptional profile. RANK signaling induces AIRE in eTACs and ILC3s (34, 35) and RANKL or other tissue/age-specific signals may shape the transcriptional and functional attributes of RORγt$^+$ DCs. RORγt$^+$ DCs may receive such signals in specific tissue niches.

RORγt-Cre lineage tracing experiments show that some cells that have previously expressed RORγt downregulate it. Although they phenotypically still resemble those cells actively expressing RORγt, these data indicate that RORγt itself may not be a good lineage defining marker. CCR6, EpCAM, CLEC4A4, and CD200 are good candidates to design a combinatorial sort strategy to identify RORγt$^+$ DCs in mice. However, RORγt is currently the most reliable marker to identify these cells by flow cytometry in mouse tissues either by using *RORγt^{GFP}* reporter mice or intracellular staining using an anti-RORC antibody. Other genes, including *PRDM16*, may be better candidates to reliably define RORγt$^+$ DCs across tissues and species. A gating strategy independent of RORγt would be critical for example in neonatal lung, where cells with *RORγt^{Cre}* expression history vastly outnumber cells with active RORγt expression. The neonatal lung is considered an environment that promotes type 2 immunity (77), while RORγt is generally associated with type 3/Th17 mediated immunity. Factors specifically expressed in neonatal lung may suppress RORγt expression, which could alter the phenotype and functions of RORγt$^+$ DCs by rendering them unresponsive to natural ligands of RORγt.

Indeed, SCENIC+ predicted RORγt itself to shape the transcriptional identity of RORγt$^+$ DCs, consistent with a recent report describing a role for RORγt in the development of Thetis cells (72). PRDM16 is a master regulator of brown fat adipogenesis that can act as transcriptional activator and repressor. Loss of PRDM16 increases γδ T17 differentiation, suggesting PRDM16 antagonizes RORγt in γδ T cells (78). GTF2IRD1, a predicted target of RORγt, can mediate the repressive action of PRDM16 (79). PRDM16 also regulates stem cell quiescence (80), raising the possibility that RORγt$^+$ DCs serve as progenitors. Indeed, RNA velocity analyses in humans suggest that RORγt$^+$ DCs may serve as alternative progenitors for cDC or ILC3-like cells (37). Although we found no evidence for that in steady-state neonatal spleen (10), the fact that cells with RORγt-expression history outnumber those with active RORγt expression would be consistent with the possibility of RORγt$^+$ DCs serving as progenitors. However, RORγt$^+$ DCs express costimulatory molecules and can activate naive T cells, indicating that they themselves constitute mature APCs. Consistent with previous reports (30), our observation that RORγt$^+$ DCs arise from lymphoid bone marrow progenitors in a Rag2-common-γ–chain-independent manner suggests that these cells are a lineage distinct from myeloid cDCs and ILC3s.

Owing to their expression of CD11c, ZBTB46, and RORγt, RORγt$^+$ DCs need to be considered in the interpretation of studies using promoters for the above genes to drive Cre or other transgenes, such as diphtheria toxin receptor. Models to specifically manipulate this cell type are urgently needed to understand its functions in immunity. However, inducible depletion models are necessary, given the necessity of RORγt$^+$ DCs for differentiating RORγt$^+$FoxP3$^+$ T regs, which regulate intestinal homeostasis and dampen type II immune responses (29, 35, 72, 73). In the absence of such models, the anti-CLEC4A4 based antigen-targeting

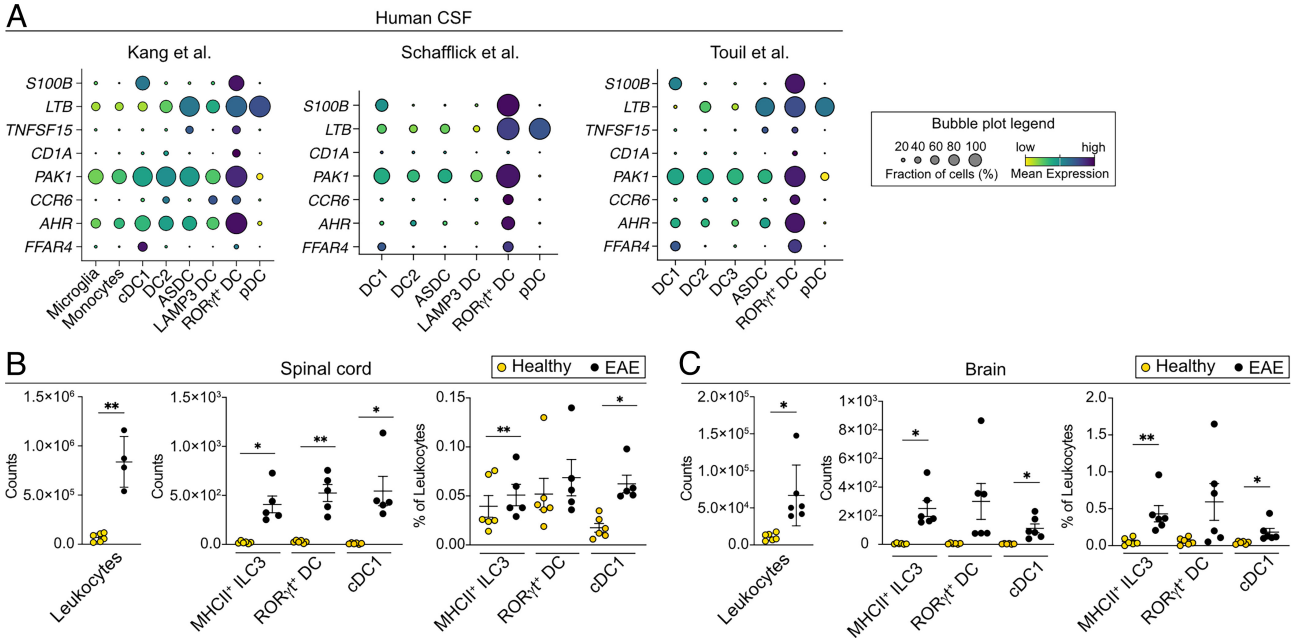

Fig. 7. RORγt$^+$ DCs in autoimmune neuroinflammation. (*A*) Bubble plots depicting expression of select genes that distinguished RORγt$^+$ DCs from other APCs in at least two of the indicated human CSF datasets. (*B* and *C*). Quantification of total leukocytes, frequency and number of MHCII$^+$ ILC3, cDC1, and RORγt$^+$ DCs in the spinal cord (*B*) and brain (*C*) of mice during peak EAE (day 16, n = 5/6) compared to healthy controls (n = 6). Each dot represents one mouse, horizontal bars represent mean, error bars represent SD. **P* (0.0332), ***P* (0.0021) ****P* (0.0002), *****P* < 0.0001. Statistical analysis was performed using two-tailed Welch's *t* test comparing cells from healthy mice vs EAE mice for each cell type. Only statistically significant comparisons are indicated.

approach used here will prove valuable to determine the specific functions of RORγt$^+$ DCs, especially compared to cDC2. RORγt$^+$ DCs also express *Ly75,* the gene encoding DEC205, suggesting they are targetable by anti-DEC205, enabling functional comparison to cDC1.

RORγt$^+$ DCs have been termed Janus cells and Thetis cells in other studies for their two-faced and shape-shifting transcriptional features and resemblance to cDCs and thymic epithelial cells. Our work shows that RORγt$^+$ DCs are indeed multifaceted in nature and bear hallmark features of DCs including the ability to integrate signals from the environment to direct appropriate immunity. Their functional versatility ranging from inducing T cell tolerance to T cell activation highlights the potential of these cells to be targeted for therapeutic applications.

Materials and Methods

Mice. Female and male age and sex-matched mice and littermate controls were housed under specific pathogen-free conditions and used in this study. All animal procedures were performed in accordance with national and institutional guidelines for animal welfare and approved by the respective authorities. See also *SI Appendix, Material and Methods*.

Cell Isolation for Flow Cytometry. Tissues were enzymatically digested; see *SI Appendix, Material and Methods*. For SI, Peyer's patches were removed only for mice 3 wk or older. mLN from 2 to 3 one-week-old mice were pooled prior to processing; mice older than 3wks were perfused with ice-cold PBS before lung isolation.

Flow Cytometry and Cell Sorting. Cells were incubated with CD16/32/FcBlock for 10 min at 4 °C and then for 30 min at 4 °C with antibodies against surface epitopes and Fixable Viability Dye eFluor 780. To preserve GFP signal after intranuclear staining, cells were prefixed with 2% paraformaldehyde at RT for 15 min. Intracellular cytokine and transcription factor staining was performed using Intracellular Fixation and Permeabilization Buffer Set and FOXP3 Transcription Factor Staining Set, respectively (both Thermo Fisher Scientific). Anti-RORC staining was performed for 1 h at RT.

Sorting: splenocytes were depleted of T cells (CD3e), B cells (CD19), Neutrophils (Ly6G), and Erythroid cells (Ter119) using magnetic beads. Cells were sorted on a BD FACSAria Fusion. Data were acquired on an LSR Fortessa (BD Biosciences) and analyzed using FlowJo V10.8.1 (Tree Star). For antibodies and further details see *SI Appendix, Material and Methods*.

In Vitro T Cell Proliferation. 250 APCs were pulsed with 10 μg/mL $OVA_{323-339}$ (Invivogen) for 3 h, washed, and cocultured with 2500 naïve CTV-labeled OTII T cells. 5 ng/mL TGF-β, 10 μg/mL anti-IL-4, and 10 μg/mL anti-IFNγ were added for Treg polarization, and 5 ng/mL TGF-β, 20 ng/mL IL-6, 10 μg/mL anti-IL-4, and 10 μg/mL anti-IFNγ for Th17 polarizing condition. 3.5 d later cells were restimulated with 10 ng/mL phorbol 12-myristate 13-acetate (PMA) (Calbiochem) and 1 μg/mL Ionomycin (Sigma-Aldrich) for a total of 5 h. Brefeldin A (BioLegend) was added during the last 3 h. See also *SI Appendix, Material and Methods*.

In Vivo Targeting. Adult RORγt^{GFP} mice were injected intraperitoneally (i.p.) with 10 μg anti-CLEC4A4-OVA or 10 μg OVA-coupled-isotype matched control antibody plus 0.2 μg/g body weight CpG-B ODN 1826 (InvivoGen). 12 h later 300 APCs were cocultured with 3000 naïve CTV-labeled OTII cells as above.

R848 Treatment. Ten-day-old *RORγt^{GFP}* mice were orally gavaged with 2 μg R848 (Invivogen) in 50μL PBS or 50μL PBS as control and analyzed 24 h later.

Single-Cell Multiomics and Transcriptomics. MHCII$^+$ ILC3, CD11c$^+$MHCII$^+$ DC, and RORγt$^+$ DCs were sorted from of 2-wk-old (P13, n = 2) and adult (8-wk-old, n = 3) *RORγt^{GFP}Clec9a$^{cre/wt}$Rosa26$^{Tom/wt}$* mice. EDTA-free buffer was used for cell isolation. For each timepoint, cells were pooled at a ratio of 1:1:10 (RORγt$^+$ DCs: MHCII$^+$ ILC3: CD11c$^+$ MHCII$^+$ DC) and nuclei isolated following the 10X Genomics Low Cell Input Nuclei Isolation protocol. 20,000 cells were lysed for 3 min on ice, resuspended in diluted Nuclei Buffer and lysis efficiency and nucleus quality assessed by trypan blue staining. 8,400 nuclei for the adult timepoint and 10,400 nuclei for the 2-wk timepoint were loaded for transposition. RNA and ATACseq libraries were prepared with the 10X Genomics Chromium Next GEM Single Cell Multiome ATAC + Gene Expression Kit and sequenced as recommended. Details of the analyses and all other transcriptomics are provided in *SI Appendix, Material and Methods*.

EAE. 12-wk-old male C57BL/6 mice were immunized subcutaneously with 250 μl of a 1:1 volume emulsion of recombinant MOG_{1-125} (400 μg) and Complete Freund's Adjuvant (Sigma). Pertussis toxin was injected i.p. on Day 0 and Day 2. Animals were scored as described in *SI Appendix, Material and Methods* and analyzed at peak disease three to five days after disease onset with mice scoring 2.5 to 3. Cell isolation from brain and spinal cord as described in *SI Appendix, Material and Methods*.

Statistics. Statistical significance was calculated in Prism 10 software (GraphPad). For pairwise comparisons two-tailed *t* test with Welch's correction was used. For multiple comparisons, one-way ANOVA with Tukey's test was performed. The Wilcoxon nonparametric ranked sum test was used to calculate differences in AUC scores in R. A P-value < 0.05 was considered significant.

Data, Materials, and Software Availability. Single-cell RNA sequencing and Multiome sequencing data have been deposited in BioStudies (S-BSST1322) (81). All study data are included in the article and/or supporting information.

ACKNOWLEDGMENTS. We thank Anne Krug and members of the Schraml lab for helpful discussions and critical reading of the manuscript. We thank members of the Krug and Dudziak laboratories, Malte Benjamin Braun, and Doğuş Altunöz for technical help, and Vasileios Bekiaris for providing *RORγt^{GFP}* mice for migration experiments. We acknowledge the Core Facilities for Flow Cytometry, Bioimaging and Animal Models at the Biomedical Center, LMU Munich for providing equipment and expertise. High-throughput sequencing was performed by the Laboratory for Functional Genome Analysis (LAFUGA) of LMU Munich. The Schraml lab is funded by an ERC Starting Grant (ERC-2016-STG-715182) and by the Deutsche Forschungsgemeinschaft (DFG, German Research Foundation) - TRR 359–Project number 491676693 (projects A01 and B05), SFB 1335/P08–Project number 360372040 and FOR2599 (Project P03, SCHR 1444/2-1). D.D. was supported by the DFG TRR 374/1 2024 TP B07 (Project number 509149993) and DU548/6-1 (Project number 431402787) and BEC by CRC1292/2-TP20 (Project Nr. 318346496) and TRR355/1-A09 (Project Nr. 490846870).

Author affiliations: [a]Institute for Immunology, Biomedical Center Munich, Faculty of Medicine, Ludwig-Maximilians-Universität in Munich, Planegg-Martinsried 82152, Germany; [b]Biomedical Center, Institute of Cardiovascular Physiology and Pathophysiology, Faculty of Medicine, Ludwig-Maximilians-Universität in Munich, Planegg-Martinsried 82152, Germany; [c]Biomedical Center, Physiological Chemistry, Faculty of Medicine, Ludwig-Maximilians-Universität in Munich, Planegg-Martinsried 82152, Germany; [d]Institute for Medical Immunology, Charité Universitätsmedizin Berlin, Corporate Member of Freie Universität Berlin and Humboldt Universität zu Berlin, Berlin 10117, Germany; [e]Section for Experimental and Translational Immunology, Institute for Health Technology, Technical University of Denmark, Kongens Lyngby 2800, Denmark; [f]Institute of Clinical Neuroimmunology, University Hospital, Ludwig-Maximilians-Universität in Munich, Planegg-Martinsried 82152, Germany; [g]Biomedical Center, Medical Faculty, Ludwig-Maximilians-Universität in Munich, Planegg-Martinsried 82152, Germany; [h]Munich Cluster of Systems Neurology (SyNergy), Munich 81377, Germany; [i]Graduate School of Systemic Neurosciences, LMU, Planegg-Martinsried 82152, Germany; [j]Molecular Medicine and Gene Therapy, Lund Stem Cell Centre, Lund University, Lund 221 84, Sweden; [k]Wallenberg Centre for Molecular Medicine at Lund University, Lund 221 84, Sweden; [l]Institute for Molecular Medicine and Research Center for Immunotherapy (Forschungszentrum für Immuntherapie), University Medical Center Johannes Gutenberg-University Mainz, Mainz 55131, Germany; [m]Institute of Medical Microbiology, Rheinisch-Westfälische Technische Hochschule Aachen University Hospital, Aachen 52074, Germany; [n]Department of Pathology and Immunology, Washington University School of Medicine, Saint Louis, MO 63110; [o]Institute of Immunology, Jena University Hospital of the Friedrich-Schiller-University, Jena 07747, Germany; [p]Immunology Section, Lund University, Lund 221 84, Sweden; [q]Calvin, Phoebe and Joan Snyder Institute for Chronic Diseases, University of Calgary, Calgary, AB T2N 1N4, Canada; and [r]Department of Microbiology, Immunology, and Infectious Diseases, Cumming School of Medicine, University of Calgary, Calgary, AB T2N 1N4, Canada

Author contributions: H.N., M.C.-T., and B.U.S. designed research; H.N., N.E.P., C.S., K.R.R., I.U., A.K., C.d.I.R., P.-Y.K., A.A., P.M., S.M., V.K., A.S., E.-L.S., J.P., and N.T. performed research; C.-F.P., L.K. and D.D., M.C., M.W.H., B.E.C., M.K., K.L., C.R. contributed new reagents/analytic tools/scientific input; H.N., M.L.R., R.S., K.R.R., and A.U.A. analyzed data; N.E.P. first observed RORγt+DCs in adult tissues; and H.N. and B.U.S. wrote the paper.

The authors declare no competing interest.

This article is a PNAS Direct Submission. H.C. is a guest editor invited by the Editorial Board.

1. M. Guilliams *et al.*, Dendritic cells, monocytes and macrophages: A unified nomenclature based on ontogeny. *Nat. Rev. Immunol.* **14**, 571–578 (2014).
2. M. Cabeza-Cabrerizo, A. Cardoso, C. M. Minutti, M. P. da Costa, C. R. Sousa, Dendritic cells revisited. *Annu. Rev. Immunol.* **39**, annurev-immunol-061020-053707-36 (2021).
3. M. Dalod, S. Scheu, Dendritic cell functions in vivo: A user's guide to current and next- generation mutant mouse models. *Eur. J. Immunol.* **52**, 1712–1749 (2022), 10.1002/eji.202149513.
4. S. K. Wculek *et al.*, Dendritic cells in cancer immunology and immunotherapy. *Nat. Rev. Immunol.* **20**, 7–24 (2020).
5. C. Lehmann *et al.*, Direct delivery of antigens to dendritic cells via antibodies specific for endocytic receptors as a promising strategy for future therapies. *Vaccines* **4**, 8–32 (2016).
6. R. Leylek *et al.*, Integrated cross-species analysis identifies a conserved transitional dendritic cell population. *Cell Rep.* **29**, 3736–3750.e8 (2019).
7. M. Alcántara-Hernández *et al.*, High-dimensional phenotypic mapping of human dendritic cells reveals interindividual variation and tissue specialization. *Immunity* **47**, 1037–1050.e6 (2017).
8. F. B. Sulczewski *et al.*, Transitional dendritic cells are distinct from conventional DC2 precursors and mediate proinflammatory antiviral responses. *Nat. Immunol.* **24**, 1265–1280 (2023), 10.1038/s41590-023-01545-7.
9. P. F. Rodrigues *et al.*, pDC-like cells are pre-DC2 and require KLF4 to control homeostatic CD4 T cells. *Sci. Immunol.* **8**, eadd4132 (2023).
10. N. E. Papaioannou *et al.*, Environmental signals rather than layered ontogeny imprint the function of type 2 conventional dendritic cells in young and adult mice. *Nat. Commun.* **12**, 464 (2021), 10.1038/s41467-020-20659-2.
11. Z. Liu *et al.*, Dendritic cell type 3 arises from Ly6C+ monocyte-dendritic cell progenitors. *Immunity* **56**, 1761–1777.e6 (2023), 10.1016/j.immuni.2023.07.001.
12. C. C. Brown *et al.*, Transcriptional basis of mouse and human dendritic cell heterogeneity. *Cell*, **179**, 846–863.e24 (2019), 10.1016/j.cell.2019.09.035.
13. M. L. Caton, M. R. Smith-Raska, B. Reizis, Notch–RBP-J signaling controls the homeostasis of CD8- dendritic cells in the spleen. *J. Exp. Med.* **204**, 1653–1664 (2007).
14. A. T. Satpathy *et al.*, Notch2-dependent classical dendritic cells orchestrate intestinal immunity to attaching-and-effacing bacterial pathogens. *Nat. Immunol.* **14**, 937–948 (2013).
15. H. Xiao *et al.*, Genomic deletion of Bcl6 differentially affects conventional dendritic cell subsets and compromises Tfh/Tfr/Th17 cell responses. *Nat. Commun.* **15**, 3554 (2024).
16. R. Tussiwand *et al.*, Klf4 expression in conventional dendritic cells is required for T helper 2 cell responses. *Immunity* **42**, 916–928 (2015).
17. K. Lutz *et al.*, Ly6D+Siglec-H+ precursors contribute to conventional dendritic cells via a Zbtb46+Ly6D+ intermediary stage. *Nat. Commun.* **13**, 3456 (2022).
18. C.-A. Dutertre *et al.*, Single-cell analysis of human mononuclear phagocytes reveals subset-defining markers and identifies circulating inflammatory dendritic cells. *Immunity* **51**, 1–26 (2019).
19. U. Cytlak *et al.*, Differential IRF8 transcription factor requirement defines two pathways of dendritic cell development in humans. *Immunity* **53**, 353–370.e8 (2020).
20. M. R. Hepworth *et al.*, Group 3 innate lymphoid cells mediate intestinal selection of commensal bacteria-specific CD4+ T cells. *Science (New York, NY)* **348**, 1031–1035 (2015).
21. F. Teng *et al.*, ILC3s control airway inflammation by limiting T cell responses to allergens and microbes. *Cell Rep.* **37**, 110051 (2021).
22. M. R. Hepworth *et al.*, Innate lymphoid cells regulate CD4+ T-cell responses to intestinal commensal bacteria. *Nature*, **498**, 113–117 (2013), 10.1038/nature12240.
23. M. Lyu *et al.*, ILC3s select microbiota-specific regulatory T cells to establish tolerance in the gut. *Nature* **610**, 744–751 (2022), 10.1038/s41586-022-05141-x.
24. L. Zhou *et al.*, Innate lymphoid cells support regulatory T cells in the intestine through interleukin-2. *Nat. Publish. Group* **12**, 1–23 (2019).
25. W. Zhou *et al.*, ZBTB46 defines and regulates ILC3s that protect the intestine. *Nature* **609**, 159–165 (2022), 10.1038/s41586-022-04934-4.
26. J. G. Castellanos *et al.*, Microbiota-induced TNF-like ligand 1A drives group 3 innate lymphoid cell-mediated barrier protection and intestinal T cell activation during colitis. *Immunity* **49**, 1077–1089.e5 (2018).
27. J. B. Grigg *et al.*, Antigen-presenting innate lymphoid cells orchestrate neuroinflammation. *Nature* **600**, 707–712 (2021).
28. J. Dobeš *et al.*, Extrathymic expression of Aire controls the induction of effective TH17 cell–mediated immune response to Candida albicans. *Nat. Immunol.* **23**, 1098–1108 (2022).
29. R. Kedmi *et al.*, A RORγt+ cell instructs gut microbiota-specific Treg cell differentiation. *Nature* **610**, 737–743 (2022).
30. B. Akagbosu *et al.*, Novel antigen-presenting cell imparts Treg-dependent tolerance to gut microbiota. *Nature* **610**, 752–760 (2022).
31. J. Abramson, J. Dobeš, M. Lyu, G. F. Sonnenberg, The emerging family of RORγt+ antigen-presenting cells *Nat. Rev. Immunol.* **24**, 64–77 (2023), 10.1038/s41577-023-00906-5.
32. G. Eberl, D. R. Littman, The role of the nuclear hormone receptor RORγt in the development of lymph nodes and Peyer's patches. *Immunol. Rev.* **195**, 81–90 (2003).
33. G. Eberl, RORγt, a multitask nuclear receptor at mucosal surfaces. *Mucosal Immunol.* **10**, 27–34 (2017).
34. T. Yamano *et al.*, Aire-expressing ILC3-like cells in the lymph node display potent APC features. *J. Exp. Med.* **216**, 1027–1037 (2019), 10.1084/jem.20181430.
35. J. Wang *et al.*, Single-cell multiomics defines tolerogenic extrathymic Aire-expressing populations with unique homology to thymic epithelium. *Sci. Immunol.* **6**, eabl5053 (2021).
36. J. M. Gardner *et al.*, Extrathymic aire-expressing cells are a distinct bone marrow-derived population that induce functional inactivation of CD4+ T Cells. *Immunity* **39**, 560–572 (2013), 10.1016/j.immuni.2013.08.005.
37. A. U. Antonova *et al.*, A distinct human cell type expressing MHCII and RORγt with dual characteristics of dendritic cells and type 3 innate lymphoid cells. *Proc. Natl. Acad. Sci. U.S.A.* **120**, e2318710120 (2023).
38. N. Torow *et al.*, M cell maturation and cDC activation determine the onset of adaptive immune priming in the neonatal Peyer's patch. *Immunity* **56**, 1220–1238.e7 (2023).
39. J. Kang *et al.*, AXL+SIGLEC6+ dendritic cells in cerebrospinal fluid and brain tissues of patients with autoimmune inflammatory demyelinating disease of CNS. *Clin. Immunol.* **253**, 109686 (2023).
40. J. Ding *et al.*, An esophagus cell atlas reveals dynamic rewiring during active eosinophilic esophagitis and remission. *Nat. Commun.* **15**, 3344 (2024).
41. B. U. Schraml *et al.*, Genetic tracing via DNGR-1 expression history defines dendritic cells as a hematopoietic lineage. *Cell* **154**, 843–858 (2013).
42. G. Eberl, D. R. Littman, Thymic origin of intestinal αβ T cells revealed by fate mapping of RORγt+ cells *Science* **305**, 248–251 (2004).
43. S. Cording *et al.*, Mouse models for the study of fate and function of innate lymphoid cells. *Eur. J. Immunol.* **48**, 1271–1280 (2018).
44. H. J. McKenna *et al.*, Mice lacking flt3 ligand have deficient hematopoiesis affecting hematopoietic progenitor cells, dendritic cells, and natural killer cells. *Blood* **95**, 3489–3497 (2000).
45. A. Baerenwaldt *et al.*, Flt3 ligand regulates the development of innate lymphoid cells in fetal and adult mice. *J. Immunol.* **196**, 2561–2571 (2016).
46. H. Spits *et al.*, Innate lymphoid cells–a proposal for uniform nomenclature. *Nat. Rev. Immunol.* **13**, 145–149 (2013).
47. C. M. Lau *et al.*, Leukemia-associated activating mutation of Flt3 expands dendritic cells and alters T cell responses. *J. Exp. Med.* **63**, jem.20150642-19 (2016).
48. R. Fiancette *et al.*, Reciprocal transcription factor networks govern tissue-resident ILC3 subset function and identity. *Nat Immunol* **22**, 1245–1255 (2021).
49. E. Lindmark *et al.*, AIRE expressing marginal zone dendritic cells balances adaptive immunity and T-follicular helper cell recruitment. *J. Autoimmun.* **42**, 62–70 (2013).
50. K. Aschenbrenner *et al.*, Selection of Foxp3+ regulatory T cells specific for self antigen expressed and presented by Aire+ medullary thymic epithelial cells. *Nat. Immunol.* **8**, 351–358 (2007).
51. A. Gayoso *et al.*, A Python library for probabilistic analysis of single-cell omics data. *Nat. Biotechnol.* **40**, 163–166 (2022).
52. T. S. Consortium *et al.*, The Tabula Sapiens: A multiple-organ, single-cell transcriptomic atlas of humans. *Science* **376**, eabl4896 (2022).
53. R. Elmentaite *et al.*, Cells of the human intestinal tract mapped across space and time. *Nature* **597**, 250–255 (2021).
54. A. R. P. Antunes *et al.*, Single-cell profiling of myeloid cells in glioblastoma across species and disease stage reveals macrophage competition and specialization. *Nat. Neurosci.* **24**, 595–610 (2021).
55. D. Schafflick *et al.*, Integrated single cell analysis of blood and cerebrospinal fluid leukocytes in multiple sclerosis. *Nat. Commun.* **11**, 247 (2020).
56. H. Touil *et al.*, A structured evaluation of cryopreservation in generating single-cell transcriptomes from cerebrospinal fluid. *Cell Rep. Methods* **3**, 100533 (2023).
57. T. K. Vogt, A. Link, J. Perrin, D. Finke, S. A. Luther, Novel function for interleukin-7 in dendritic cell development. *Blood* **113**, 3961–3968 (2009).
58. A. Weckel *et al.*, Long-term tolerance to skin commensals is established neonatally through a specialized dendritic cell subgroup. *Immunity* **56**, 1239–1254.e7 (2023).
59. C. B. González-Blas *et al.*, SCENIC+: Single-cell multiomic inference of enhancers and gene regulatory networks. *Nat. Methods* **20**, 1355–1367 (2023).
60. M. J. Harms *et al.*, PRDM16 binds MED1 and controls chromatin architecture to determine a brown fat transcriptional program. *Genes Dev.* **29**, 298–307 (2015).
61. P. Seale *et al.*, PRDM16 controls a brown fat/skeletal muscle switch. *Nature* **454**, 961–967 (2008).
62. N. von Burg *et al.*, Activated group 3 innate lymphoid cells promote T-cell–mediated immune responses. *Proc. Natl. Acad. Sci. U.S.A.* **111**, 12835–12840 (2014).
63. D. Dudziak *et al.*, Differential antigen processing by dendritic cell subsets in vivo. *Science (New York, NY)* **315**, 107–111 (2007).
64. A. G. López *et al.*, Migration of murine intestinal dendritic cell subsets upon intrinsic and extrinsic TLR3 stimulation. *Eur. J. Immunol.* **50**, 1525–1536 (2020).
65. F. Michetti *et al.*, The S100B protein: A multifaceted pathogenic factor more than a biomarker. *Int. J. Mol. Sci.* **24**, 9605 (2023).
66. S. Columba-Cabezas *et al.*, Suppression of established experimental autoimmune encephalomyelitis and formation of meningeal lymphoid follicles by lymphotoxin β receptor-Ig fusion protein. *J. Neuroimmunol.* **179**, 76–86 (2006).
67. B. P. Pappu *et al.*, TL1A–DR3 interaction regulates Th17 cell function and Th17-mediated autoimmune disease. *J. Exp. Med.* **205**, 1049–1062 (2008).
68. A. Liston *et al.*, Inhibition of CCR6 function reduces the severity of experimental autoimmune encephalomyelitis via effects on the priming phase of the immune response. *J. Immunol.* **182**, 3121–3130 (2009).
69. C. Feng *et al.*, Docosahexaenoic acid ameliorates autoimmune inflammation by activating GPR120 signaling pathway in dendritic cells. *Int. Immunopharmacol.* **97**, 107698 (2021).
70. C. Gutiérrez-Vázquez, F. J. Quintana, Regulation of the immune response by the aryl hydrocarbon receptor. *Immunity* **48**, 19–33 (2018).
71. M. Gargaro *et al.*, Indoleamine 2,3-dioxygenase 1 activation in mature cDC1 promotes tolerogenic education of inflammatory cDC2 via metabolic communication. *Immunity* **55**, 1032–1050.e14 (2022).
72. L. Fu *et al.*, RORγt-dependent antigen-presenting cells direct regulatory T cell–mediated tolerance to food antigen. bioRxiv [Preprint] (2024), 10.1101/2024.07.23.604803 (Accessed 20 August 2024).
73. A. Rudnitsky, H. Oh, J. Talmor, R. Kedmi, Coordinated network of T cells and antigen presenting cells regulate tolerance to food. bioRxiv [Preprint] (2024), 10.1101/2024.07.11.603064 (Accessed 20 August 2024).
74. Y. F. Parisotto *et al.*, Thetis cells induce food-specific Treg cell differentiation and oral tolerance. bioRxiv [Preprint] (2024), 10.1101/2024.05.08.592952 (Accessed 20 August 2024).
75. J. L. Gommerman, J. L. Browning, C. F. Ware, The lymphotoxin network: Orchestrating a type I interferon response to optimize adaptive immunity. *Cytokine Growth Factor Rev.* **25**, 139–145 (2014).
76. L. Zeitler, P. J. Murray, IL4i1 and IDO1: Oxidases that control a tryptophan metabolic nexus in cancer. *J. Biol. Chem.* **299**, 104827 (2023).
77. I. M. de Kleer *et al.*, Perinatal activation of the interleukin-33 pathway promotes type 2 immunity in the developing lung. *Immunity* **45**, 1285–1298 (2016).
78. J. Nah, Y. Lee, R. H. Seong, PRDM16 regulates γδT17 cell differentiation via controlling type 17 program and lipid-dependent cell fitness. *Front. Immunol.* **14**, 1332386 (2024).
79. Y. Hasegawa *et al.*, Repression of adipose tissue fibrosis through a PRDM16-GTF2IRD1 complex improves systemic glucose homeostasis. *Cell Metab.* **27**, 180–194.e6 (2018).
80. K. O. Gudmundsson *et al.*, Prdm16 is a critical regulator of adult long-term hematopoietic stem cell quiescence. *Proc. Natl. Acad. Sci. U.S.A.* **117**, 31945–31953 (2020).
81. H. Narasimhan, M. Richter, B. Schraml, Data from "RORγt-expressing dendritic cells are functionally versatile and evolutionarily conserved antigen presenting cells". Biostudies. http://www.ebi.ac.uk/biostudies/studies/S-BSST1322. Deposited 31 January 2025.